Dryline on 22 May 2002 During IHOP:

Convective Scale Measurements at the Profiling Site

Part-I

BELAY DEMOZ[1], CYRILLE FLAMANT[2], DAVID MILLER[3], KEITH EVANS[4], FRÉDÉRIC FABRY [5], PAOLO DI GIROLAMO[6], DAVID WHITEMAN[1], BART GEERTS[7], TAMMY WECKWERTH[8], WILLIAM BROWN[7], GEARY SCHWEMMER[1], BRUCE GENTRY[1], WAYNE FELTZ[9], ZHIEN WANG[4]

[1]NASA Goddard Space Flight Center, Greenbelt, MD, 20771
[2]CNRS Service Aeronomie, Paris, France
[3]Science Systems and Applications, Inc., Lanham, MD, 20706
[4]University of Maryland-Baltimore County, Baltimore, MD, 21228
[5]McGill University, Montreal, Canada
[6]Università degli Studi della Basilicata, Potenza, Italy
[7]University of Wyoming, Laramie, WY 82071
[8]National Center for Atmospheric Research, Boulder, CO 80307-3000
[9]CIMSS/SSEC - University of Wisconsin – Madison, Madison, Wisconsin 53706

To be Submitted to Monthly Weather Review (IHOP Special Issue)

15 August, 2004

Corresponding author: Belay B. Demoz, NASA/GSFC, Code 912, Greenbelt, MD 20771
Tel : 301-614-6224, Fax: 301-614-5492, Email: Belay.B.Demoz@nasa.gov

ABSTRACT

A unique set of measurements of wind, water vapor mixing ratio and boundary layer height variability was observed during the first IHOP dryline mission of 22 May 2002. Water vapor mixing ratio from the Scanning Raman Lidar (SRL), high-resolution profiles of aerosol backscatter from the HARLIE and wind profiles from the GLOW are combined with the vertical velocity derived from the NCAR/ISS/MAPR and the high-resolution FMCW radar to reveal the convective variability of the cumulus cloud-topped boundary layer. A combined analysis of the in-situ and remote sensing data from aircraft, radiosonde, lidars, and radars reveals moisture variability within boundary layer updraft and downdraft regions as well as characterizes the boundary layer height variability in the dry and moist sides of the dryline. The profiler site measurements will be tied to aircraft data to reveal the relative intensity and location of these updrafts to the dry line. This study provides unprecedented high temporal and spatial resolution measurements of wind, moisture and backscatter within a dryline and the associated convective boundary layer.

1. INTRODUCTION

The dryline occurs in the mid-west of the US and is sometimes called a "dew point front" or "dry front." It is a boundary between warm, moist air that originated from the Gulf of Mexico and hot, dry air from the Mexican Plateau and southwest desert. It is sometimes a favored zone for initiation of severe weather (Rhea, 1966). Dryline moisture differences and sharpness (Fujita 1958; NSSP Staff 1963), dryline characteristics and motion (Schaefer, 1986; Parsons et al. 1991), potential for convection (Blustein and Parker, 1993), and vertical mixing (Zeigler and Hane, 1993) have been reported. These studies have also shown that the mere presence of a dryline does not imply occurrence of deep convection, although, cumulus and cumulus congestus clouds are frequently observed. The flow along the dryline is dominated by convective-scale processes (Ziegler and Hane, 1993) but there are still outstanding questions on how storms initiate along the dryline and what the source of the convergence is that initiates clouds and storms along the dryline (Parsons et al. 2000; Ziegler and Hahn, 1993; Sun and Ogura, 1979; Schaefer, 1986). As outlined by Parsons et al (2000), our knowledge is also lacking on the variability of the strength of the moisture gradient and convergence variations with diurnal cycle.

In this paper, we focus on the quantification of the small-scale variability of boundary layer parameters, key to understanding convective initiation. The variability in the convective boundary layer moisture, wind and temperature fields and their importance in the initiation of storms have been discussed in the literature (Weckwerth et al., 1996; Crook, 1986 and Weckwerth, 2000). These variations have been reported in relation to frontal zones, stationary boundaries and within horizontal convective rolls (see Weckwerth et al. 1996 for a discussion and references). While all three fields (temperature, wind and moisture) vary

substantially in the convective boundary layer, moisture poses a particular challenge. It presents a unique measurement challenge because water vapor content can vary by more than three orders of magnitude in the troposphere and can suffer from large sampling errors and substantial variability both in the vertical and horizontal. Thus, characterization of high resolution 3D-distribution of water vapor is very difficult. However, it has many advantages in visualizing many of the dynamic features. Water vapor concentration (expressed as a mass mixing ratio, g kg^{-1}), is conserved in all meteorological processes except condensation and evaporation and often remains distinct across an air-mass boundary even when the temperature difference is minimal.

This paper will focus on the evolution and variability of the convective scale moisture and wind in the boundary layer during a dry line event that occurred on 22 May 2002 during the International H_2O Project (IHOP_2002). IHOP is a field experiment that took place over the Southern Great Plains (SGP) of the United States from 13 May to 30 June 2002. The main goal of IHOP is to improve characterization of the four-dimensional (4-D) distribution of water vapor and evaluate its use in improving the understanding and prediction of convection. Instrumented mobile vehicles, aircraft, radars (fixed and mobile), mobile radionsonde launches, meso-networks, lidars and a suit of other ground-based instrumentation were operational during IHOP and on 22 May 2002 in the Oklahoma Panhandle. Weckwerth et al (2004) provide a full discussion of the observational network, measurement strategy and instruments deployed during IHOP. Of primary importance for the discussion in this paper are i) the National Center for Atmospheric Research's (NCAR) Integrated Sounding System (ISS) which consisted standard surface meteorology station, a sodar, a radiosonde station, and a UHF wind profiler referred to as MAPR/ISS (Multiple Antenna Profiler Radar profiler), ii) the three NASA Goddard Space Flight Center (GSFC) ground based lidars for remote sensing

of water vapor, aerosol backscatter, and wind profiles, iii) the University of Massasuchets frequency modulated continuous-wave (FMCW) radar, iv) the University of Wisconsin Atmospheric Emitted Radiance Interferometer (AERI), and other standard meteorological instruments at the Homestead Profiling Site in the Oklahoma panhandle. In particular, the focus here is on the three GSFC lidars: the Scanning Raman Lidar (SRL), the Goddard Laboratory for Observing Winds (GLOW), and the Holographic Airborne Rotating Lidar Instrument Experiment (HARLIE).

Synthesis of all aspects of the data collected on 22 May 2002 and IHOP is ongoing and is reported by others in *this issue*. This discussion will be limited to profiler observations of the convective scale plumes and boundary layer variability on 22 May 2002 over the IHOP profiler site in the Oklahoma Panhandle (referred to here as Homestead). The analysis in this work is unique in that it combines simultaneous, lidar-based measurements of wind, moisture and Convective Boundary Layer (CBL) structure with many measurements from aircraft, radar, profiler, and profiles of infrared moisture and temperature and other data to study thermodynamic variability in and around clear air updrafts during a dryline event. Variations of the moisture plumes as the dryline moved back and forth over the ground site are observed and the site specific profile observations are related to the larger picture using aircraft and radar based measurements.

A brief description of the synoptic setting using satellite, sonde and radar data is presented in section 2. Many of the profiler instruments at Homestead are relatively new and information on their performance may not be easily accessible. Thus, in section 3, a brief discussion of the Homestead-based instruments and their measurements on 22 May 2002 are presented.

Analysis and synthesis of the data and supporting evidence from aircraft observations on the day are presented in section 4. A summary and some conclusions are presented in section 5.

2. SYNOPTIC SETTING

2.1. Satellite data

Satellite and surface analysis indicated that starting about 1600 (all times UTC) there was an approaching cold front over the Northern High plains with a strong south-southwesterly flow ahead. At the same time, the Southern Plains were under a southerly flow and a stratocumulus layer was visible in much of eastern Oklahoma and east of the observed dryline that was located just west of the Homestead area, in the Oklahoma Panhandle and oriented roughly north-south. By about 2100, GOES visible imagery revealed a "wedge" shaped area of cumulus clouds oriented roughly NNE-SSW that extended from the Texas Panhandle into northwest Kansas (Fig. 1). The Cu clouds appeared stationary and were visible in GOES maps until about 0030. At about the same time, convection was triggered in southwestern Kansas at the apparent triple point – where the dryline (identified by the Cu clouds) and approaching front merged. Much of the IHOP aircraft and mobile ground instrumentation discussed in this paper occurred well south of this triple point – near the location of the site for the National Center for Atmospheric Research Polarization radar (S-pol) and Homestead.

2.2. Time series data at Homestead

Surface observations of temperature, wind, relative humidity, and precipitable water vapor at Homestead between 1500 on 22 May and 0600 on 23 May 2002 are plotted in Fig. 2. Surface wind direction varied between southwesterly and south-southeasterly during the entire day,

typical during dryline conditions (Schaefer, 1973). Wind speeds were between 13-15 m/sec, on the average with values as low as 10 m/sec at 1200 (not shown), just prior to the start of a steady increase in precipitable water vapor amounts – indicating arrival of the moist air over Homestead. The dryline on this date started as a broad, diffuse "region" of moisture with increases in dew point temperature and precipitable water vapor observed starting around 1600. Dew point temperatures around 1900 were approximately 10 ^{0}C at Homestead dropping to -5 ^{0}C in Guymon, OK, about 30 miles to the west. Temperature and relative humidity records show the general diurnal trend, warming and drying in the afternoon followed by cooling and humidity increase in the evening. Superimposed in this diurnal trend, however, are two dry regions centered about 1700 and 2200 UTC. These times are characterized by a distinct dry airmass, as manifested in the moisture and to a smaller degree in the temperature measurements. Mixing ratio values were, on the average, about 9 g/kg between 1200 and 2400, except around 1700 and 2200 when mixing ratio values decreased to about 8 and 7 g/kg, respectively.

The 1700 moisture dip was associated with the start of the increase in PWV values and most probably a sign of the initial arrival of the dryline. However, most of the lidar profilers at Homestead became operational hours later –limiting our discussion to the later dip at 2200. A detailed look at the surface measurements between 2000 and 0100 revealed that the 2200 dip was composed of several oscillations of distinct moisture (relative humidity) and temperature regions about 10 minutes long in duration. Within the 2200 dip, the wind direction was generally from the southwest (driest section has a direction of 200 degrees) with a sinusoidal character, of peak-to-peak distance of about 1-1.5 hrs until 2300, but composed of several "pockets" of smaller scale oscillations (~5-10 minutes wide). At an average wind speed of 15 m/sec, the organization suggests 4 - 8 km wide distinct air pockets

populating mostly the dry intrusion at 2200. The same scales of organization are also seen in the refractivity plot, contributed mainly through the moisture (wet) term, in the same range as the scales found in section 2.2 below from Spol measurements. The drying at 2200 and the associated oscillations occurred as part of a larger scale oscillation of the dryline over Homestead discussed below.

2.3 Sounding data

Several sounding units participated on this day. A Lear Jet dropped eight dropsonde packages along a line from just east of Homestead to central Oklahoma, near the Atmospheric Radiation Measurement (ARM) site (see Fig. 1). Mobile sounding units from NCAR and the National Severe Storms Laboratory (NSSL) respectively launched GLASS and CLASS (Bluestein, 1993) sondes at and around Homestead. Figure 3 shows plots of soundings made from locations slightly west and east as well as at Homestead. The sounding from the western location was characterized by very dry boundary layer, almost no convective available potential energy (CAPE=0; CIN =-42 J/kg), low dew point temperatures at the surface and decreasing rapidly with altitude. At stations in the immediate east, the airmass was characterized by appreciable CAPE (CAPE=1281 J/kg; CIN=-214 J/kg) higher dew point temperatures at low levels and an abrupt drying of the air above. Dropsondes released further east showed increased water vapor mixing ratio amounts at lower levels leading to a sharper contrast with the overlying dry air mass. Compared to the air west of Homestead, the low level moisture was substantial. For example, at 890 m MSL, the dew point changed from 0.3°C in the west to 12.1°C in the immediate eastern side of Homestead.

An east-west cross-section of sondes launched between 2130 and 2239 is shown in Fig. 3b. The figure covers the region from about 20 miles west of Homestead to about the ARM site

(Fig. 1). Note that since the contour is constructed from data that span about 1-hour, "shorter term" waves and changes introduced by BL evolution occurring within the time duration are excluded. Potential temperature (K – dark lines) and mixing ratio (g/kg – dash lines) and wind barbs are plotted.

The mixing ratio changes from dry to the west of S-pol (< 5 g/kg) to more than 12 g/kg in western-central Oklahoma. In the eastern half of the fig (L4-L8), a well defined moisture depth is observed. Over Homestead, a deeper lofting of the moisture contours was observed - an indication of vigorous vertical mixing of moisture to about 3.5 km altitude coincident with the observation of cumulus clouds (Fig.1).

2.4 NCAR S-Pol data

An in depth analysis of the methods, data products, and S-pol measurements during IHOP and on this day are detailed elsewhere (e.g. see Weckwerth et al, 2004; Fabry, 2004). S-pol data are presented here to show the "vacillation" of the dryline about Homestead and to understand the relative location of Homestead-based analysis vis-à-vis the larger scale picture of the dryline conditions. Refractivity data were retrieved whenever 0° elevation surveillance scans were made by S-Pol, typically done every 5 minutes.

Figure 4 is a plot of near surface reflectivity, refractivity, 5-min refractivity changes and a time series of refractivity calculated from surface measurements as well as SRL and AERI (discussed later) data at Homestead (black dot in the refractivity change figure) given for comparison purposes. A more thorough IHOP refractivity intercomparison can be found in Weckwerth et al. (2004). The time sequence plots of the S-Pol refractivity show that the cool moist airmass of higher refractivity (blue area) being pushed east and replaced by SSW-NNE

wedge shaped warm/dry air from the southwest (green area) before moving back west again over Homestead, consistent with the wind direction indicated. Homestead was under a cool/moist air at 2100 with the dry air taking hold around 2140 from NNW and persisted until about 2220 (Fig. 4 – bottom) before being replaced again by the cool/moist airmass from the southwest. Note that, using an average surface wind speed of 14-15 m/sec, this translates to about 18-20 km wide dry/warm air intrusion – about the same distance between the edges of the cumulus field (Fig. 1), at the latitude of Homestead. The reflectivity field (Fig. 4, top) revealed two reflectivity fine lines corresponding to the edges of the NNE-SSW oriented wedge-shaped warm/dry airmass – suggesting a "double dryline" feature, the stronger echo associated with the eastern boundary. These lines became more distinct in the latter hours of the afternoon (2300 – 0000) when the relative difference between refractivity in the dry/warm region to the west and the moist/cool region to the east increased. The boundaries, in particular the eastern boundary, were not straight N-S lines but had E-W wiggles of few kilometers in amplitude that may have caused the observed oscillations in refractivity and moisture at Homestead between 2130 and 2320. The associated 5-minute refractivity changes revealed a range of smaller scale organizations (2-5 km across and up to 10 km along the dryline) of dryline and moist cells (blue and red, respectively) dominated the boundaries.

A movie of the complete 5-minute data for this day revealed that the fine lines moved east far enough for the eastern boundary (the main dryline) to reach slightly past Homestead, allowing for an excellent sampling of the vertical structure of the wedge shaped airmass and its transition to the cool/moist airmass by the lidar/radar profilers (section 3). First, a discussion of supporting aircraft measurements showing the double dryline observations and a regional view of the eastern and western dryline convergence zones will be made.

2.5 Supporting Aircraft Observations

a. In-situ moisture and vertical velocity data

Many of the features reported in the profiler data at Homestead were also observed in the aircraft data collected on 22 May 2002. The University of Wyoming King Air (UWKA) research aircraft and the Naval Research Laboratory P3 aircraft (P3), in addition to the Lear jet described above, were operational around Homestead. Presenting a full scale analysis of the data from the aircraft is beyond the scope of this manuscript. However, selected legs and data in support of the analysis are presented here.

Figure 5, shows the time series of in-situ water vapor mixing ratio and vertical velocity of wind data from a flight leg at 1.6 km MSL. The flight leg was oriented NNW-to-SSE, located slightly north of Homestead. Three distinct regions of water vapor mixing ratio values are evident: 8-9 g/kg in the southeast section of the leg, an average of 6 g/kg region in the middle and a drier region (4 g/kg) in the northwest. These two "jumps" in the mixing ratio structure (about 16 -18 km apart) correspond to the double dryline features discussed earlier (Figs. 4). The water vapor mixing ratio change in the western bump associated with the faint radar reflectivity line in Fig. 4 was about 2 g/kg while the change associated with the stronger reflectivity line was 3 g/kg. The area in the immediate west (~ 6km or flight of 1 minute) of the eastern dryline was warmer by about 1 ^{0}C (not shown) and had an average vertical velocity of 1.6 m/sec compared to the immediate area in the moist side. For the western dryline, the average vertical velocity and temperature were near zero. These differences have important implications on the maintenances and structure of the dryline (see Ziegler and Hane, 1993).

The associated UWKA vertical velocity data in Fig. 5 show that the vertical velocity in the moist part of the leg was less intense than the drier side. The same conclusion is reached when considering the entire UWKA flight legs on this day (not shown here). In addition, the scale of the updrafts and downdrafts was composed of small scale perturbations (1 km or less) superimposed on larger scale (4-5 km) bumps. The latter is the scale identified in the FMCW and SRL plumes discussed earlier. The vertical velocities varied between -3 m/sec and 3 m/sec, in general, with an average for the flight leg of -0.5 m/sec. Note that the UWKA vertical velocity measurements are believed to be accurate to at least 0.5 m s^{-1} for instantaneous measurements and to at least half that, possibly to 0.1 m s^{-1}, for long-track averages (Geerts and Miao, 2004). These observations are similar to those observed by the MAPR but less than the reported values by Weiss et al. (2004).

Across dryline moisture variability measurements onboard the NRL P-3

During IHOP_2002 CI missions, the Naval Research Laboratory (NRL) P-3 aircraft was dedicated to the documentation of along and across dryline thermodynamical characteristics using both remote sensing and in situ measurements. Remote sensing instruments included the airborne water vapor differential absorption lidar (DIAL) LEANDRE 2 (or L2) and the airborne Doppler radar ELDORA/ASTRAIIA. The NRL P-3 sampling strategy was the following: the NRL P-3 flew long east-west survey legs in the region of Homestead (were the convection was forecasted to initiate), in order to detect boundaries/drylines. Upon detecting the boundaries D1 and D2, the NRL P-3 flew elongated box patterns around boundary D1 (which was better defined than boundary D2 at the time of the survey), the longest dimension of the box being parallel to the dryline.

In this section, we examine the horizontal variability of moisture field in the PBL as observed by L2 on 22 May 2002 along one of the early east-west survey legs. Horizontal pointing DIAL measurements made in the framework of IHOP_2002, provided the first ever observations of the horizontal structure of the water vapor field in the vicinity of drylines. The operation of non-eye safe L2 in horizontal mode required the support of an aircraft-proximity radar and careful flight planning (see Weckwerth et al., 2004; for further details). The details concerning the design of the LEANDRE 2 system and the standard DIAL signal processing are given in Bruneau et al. (2001).

The two-dimensional horizontal structure of the water vapor field measured by L2 at 1.2 km AGL across the boundaries D1 and D2 between 2037 and 2056 is shown in Fig. 6a. A gap (approximately 25 km of a 125 km long leg) is observed in the L2 data which results from an unfortunate L2 operator maneuver. The along track resolution is 5 s which translates to a spatial resolution of 0.7 km (assuming an aircraft speed of 140 m/s). As discussed in Bruneau et al. (2001), L2 water vapor mixing ratio retrievals have a precision better than 0.5 g kg^{-1} within a 5 km distance from the aircraft and an along-beam resolution of 300 m. In the configuration for the 22 May operation, reliable retrievals of water vapor mixing ratio were obtained at distances ranging from 1.2 to 2.7 km from the aircraft; saturation of the lidar signal at close range and attenuation at far range limiting data quality (see details in Murphy et al. this issue). The probable locations of the dryline convergence zones and associated regions are marked accordingly in the figure. Homestead (longitude -100.6) was located just east of the eastern dryline (D1).

Figure 6b shows a comparison of the water vapor mixing ratio measured in-situ by the NRL P-3, and the L2 data range averaged data between 1.35 and 2.25 km from the aircraft.

Excellent agreement is found between the two curves. Three distinct regions are identified from the water vapor mixing ratio evolution on the east-west NRL P-3 transect. East of D1 (located around -100.8°E, i.e. east of Homestead at 2047), water vapor mixing ratios are comprised between 8 and 10 g kg^{-1}. West of D1, a sharp decrease is observed, with water vapor mixing ratios in the range of 5-6 g kg^{-1} till about D2; located at approximately -101.1°E. The water vapor mixing ratio gradient across D2 dropped again to the west by about 1 g kg^{-1} – a much weaker drop than that across D1 (3 g kg^{-1}). West of D2, water vapor mixing ratio values were between 4 and 3 g kg^{-1}. East of the eastern dryline (D1), the water vapor mixing ratio values were similar to that measured by in-situ UWKA instruments almost three hours later (2333-2339) while to the west of D1, the airmass was slightly drier at the time of the NRL P-3 passage.

3. Data sources at Homestead and analysis techniques

a. The Goddard Lidar Observatory for Winds (GLOW)

The Goddard Lidar Observatory for Winds (GLOW) is a mobile Doppler lidar system which uses direct detection Doppler lidar techniques to measure wind profiles from the surface into the lower stratosphere (Gentry 2000). The lidar system uses a Nd:YAG laser transmitter to measure winds using either aerosol backscatter at 1064 nm or molecular backscatter at 355 nm. The receiver telescope is a 45 cm diameter Dall-Kirkham which is fiber coupled to separate Doppler receivers, one optimized for the aerosol backscatter wind measurement and another optimized for the molecular backscatter wind measurement. The receivers are implementations of the 'double edge' technique and use high spectral resolution Fabry-Perot etalons to measure the Doppler shift. Because of logistical reasons, only the molecular reciever was operational during IHOP. A 45 cm aperture azimuth-over-elevation scanner is

mounted on the roof of the van to allow full sky access and a variety of scanning options. The GLOW molecular receiver has been designed for efficient operation in the clear air regions of the free troposphere and lower stratosphere. This provided some challenges for IHOP which was focused on convective activity in the boundary layer and lower troposphere. The photon counting photomultiplier tube detectors provide high detection sensitivity in the upper troposphere and stratosphere where the return signals are small. One side effect of this is that when the maximum laser pulse energy and the full telescope aperture are used the signals collected from ranges less than 5 km are too large and the response of the photon counting detectors is non-linear. To ensure coverage of the lowest 5 km the signal levels were optimized by reducing the pulse energy to between 5 mJ and 40 mJ. In addition, the effective telescope aperture was reduced from 45 cm to 25 cm.

GLOW measurements of wind speed and direction on 22 May 2002 are shown in Fig. 7. The wind profile measurements plotted are at 10 minutes and 100 m vertical resolution in time and space, respectively. The lidar wind measurement accuracy is range dependent. For the profiles shown in Figure 7, the error does not exceed 3 m/s and is considerably smaller at lower altitudes. The data gap between 2200 – 2330 was a result of sector scan operation mode - made at several elevation angles to ascertain variations in dryline associated flows (not shown). These data are not fully analyzed but a preliminary analysis does not add any new findings to the present study.

The prevailing wind early on 22 May 2002 was from the southwest, changing to southerly after about 2300. A shift from southerly to southeasterly after about 2330 at heights of about 1 km and lower is also consistent with past observations of wind evolution in a dryline environment in this area (Schaefer, 1986). Wind speeds below 0.5 km were generally about

15 m/s, increasing with altitude, reaching up to 25-30 m/s by 2-3 km. An interesting evolution of the wind direction and speed with altitude is observed between 2330 and 0100: the depth of the southeasterly air gradually increased to about 1 km while at the same time wind speed values decreased in an eastward-tilted vertical region of about 1.5 km in depth followed by an increased wind speed region. This structure, tilted slope airmass with increased wind following, has similarities with the "nose" of a density current structure see Atkins et al. 1998) and may signify the result of a convergent zone which led to observations of mesovortices around Homestead, discussed elsewhere (see Buban et al., 2004 – this issue).

b. The Holographic Airborne Rotating Lidar Instrument Experiment (HARLIE)

HARLIE (Schwemmer, G.K., 1998) is a scanning aerosol backscatter lidar that for IHOP was deployed in a ground-based trailer to perform continuous azimuth scans along an inverted cone having a vertically pointing rotation axis. The HARLIE transceiver telescope is a 40 cm diameter transmission holographic optical element (HOE) that collimates and scans the transmitted laser beam and collects and focuses the atmospheric backscatter. The Nd:YAG laser transmits 1064 nm wavelength, 200 μJ pulses at a 5 kHz repetition rate. The receiver accumulates photo-counts in 30 m range bins, producing profiles of backscatter for 500 shots, every 100 ms. The HOE has a 45-degree diffraction angle and rotates continuously in azimuth during operation resulting in a conical scan of regard and 20 m vertical sampling. Scan rates between 0-30 rpm are possible, but for most of the IHOP experiment a scan rate of 30 degrees/second (12 second scan period) was used which yields a 3 degree azimuth resolution. The instrument can also be tipped at 45 degrees and kept pointed in a fixed direction so that conventional vertical pointing measurements can be obtained. The scanning data provides a pseudo-3D visualization of aerosol backscatter, and principal data products include aerosol backscatter profiles, cloud boundary and heights, boundary layer heights and

entrainment zone thickness. In addition, coherent structures in the backscatter field can be tracked as they progress across the conical scan surface, resulting in an estimation of the wind speed (Wilkerson et.al., 2001).

HARLIE measurements of range normalized log backscatter on 22 May 2002 are shown in Fig. 8. Between 2030 and 2140 hours HARLIE was used in a vertical pointing, non-scanning mode. After the short gap in the data at 2140 h, HARLIE was used in the normal conical scanning mode for the rest of the day. The scanning data are averaged over each scan to produce a vertical profile on this image every 12 seconds. The color bar covers 3 decades of backscatter values, with yellow and white values indicating visible clouds. Stippling in the image at higher altitudes is due to noise from the daytime solar background, which increases at higher altitudes due to the range squared correction applied to the signal. The mean background values are subtracted from the measured signals. Development of the BL and clouds and the subsequent nighttime drop in the BL height is well resolved. During most of the morning and afternoon, surface heating causes the lifting and mixing of the low level moist air with dry air aloft, leading to the development of the BL which reached heights of 3 to 3.5 km and subsequent clouds. This mixing is suggested by the growing backscatter "plumes" observed mostly prior to sunset (about 0140). Note that the semblance of a continuous cloud deck after 2140 (Fig. 8) is an artifact of the scan averaging used here. BL height and spatial variability derived from HARLIE is discussed below.

c. The Scanning Raman Lidar (SRL)

The SRL is a mobile lidar system contained in a single environmentally controlled trailer. It is based on a tripled Nd:YAG laser (354.7 nm), 0.76 meter horizontally mounted telescope, 1.1 x 0.8 m flat mirror enabling full aperture scanning of the telescope in a single scan plane

and combined photon counting and analog-to-digital data acquisition system. Using Raman scattering from atmospheric molecules, the lidar system measures high temporal and spatial resolution profiles of the traditional quantities of aerosol backscattering, extinction, and water vapor mixing ratio during both daytime and nighttime. Cloud base height information is also easily derived (Demoz et al., 2000). Details about the Raman technique and examples of water vapor and aerosol measurements using Raman lidar can be found in (Whiteman et. al, 1992 and Whiteman et. al., 2001). An updated analysis of the narrow-band Raman lidar configuration used for the IHOP field campaign can be found in (Whiteman 2003 a,b). For the IHOP field deployment, the SRL underwent an extensive set of hardware modifications that added a 0.25m telescope to the system providing low altitude channels and aerosol depolarization measurements. In addition, separate cloud liquid water channels (Whiteman and Melfi, 1999) were added to the system. As an experimental configuration for IHOP, rotational Raman temperature measurements were also added to the SRL (Di Girolamo et. al. 2003).

The SRL measured water vapor mixing data on 22 May 2002 is shown in Fig 9. The data was acquired from ~2000 on May 22 until ~0300 on May 23; approximately 3 hours after solar noon until approximately 3 hours after sunset. The evolution of water vapor mixing ratio, development of the afternoon CBL and subsequent cloud development (seen as white vertical stripes between 2200 and 2400; a result of complete attenuation of the laser beam) is detailed. Also shown is the vertical profile evolution of the water vapor mixing ratio during a dryline. The afternoon convection mixed the moisture to higher and higher altitudes reaching as high as 3.4 km (cloud base) above ground. Starting a little before sunset, the vertical mixing diminished and a better distinction of the dryline and the overlying airmass boundaries start to emerge.

As discussed above, between 2130 and 2230, Homestead was under the "wedge' shaped airmass bounded by the two dryline convergence zones. The SRL data in this region (Fig 9) reveals that the airmass was characterized by a well-mixed CBL of water vapor mixing ratio values of about 6 g/kg through most of the BL. The mixing ratio values increase to 9-10 g/kg in the eastern dryline convergence zone and the BL was characterized by convective plumes of moist air reaching up to about 2.5 km altitude. Note also that the shape of the 9-10 g/kg (red-yellow transition) between 2330-0100 coincides and resembles the eastward tilt observed in the GLOW measured wind speeds.

The data shown in Fig.9 were smoothed with a three-minute running window resulting in approximately 2-minute temporal resolution as determined by Fourier spectral analysis. In addition, variable vertical smoothing was used resulting in the following resolutions: <1km: 60 m resolution, 1-2km: 100 m, 2-3km: 150m, 3-4km: 190m, >4km: 210m. This averaging scheme was used to minimize errors introduced due to the effect of daytime background light in the data. Note that even though the SRL uses a combination of narrow spectral band pass and narrow telescope field of view (NFOV) technique to reduce the amount of solar background noise, it is still influenced by changing background light levels. Nonetheless, it permits high-resolution daytime water vapor measurements to the top of the boundary layer while permitting nighttime measurements to the tropopause. The random error in the SRL mixing ratio data is 10% or less in the boundary layer during the daytime but increases rapidly above the boundary layer due to drier conditions found there. Under nighttime conditions, the random error is less than 2% in the boundary layer and reaches 10% at 6 km. Longer averaging times permit measurements to extend to the upper troposphere during the nighttime.

e. The Frequency Modulated Continuous-Wave (FMCW) Radar

The University of Massachusetts frequency modulated continuous-wave (FMCW) radar system was also deployed during IHOP_2002 and was located at Homestead side by side with the SRL, HARLIE, GLOW, AERI and MAPR. The radar operates at S-band (2.9 GHz) with a 2.5 m vertical resolution and a 45 ms temporal resolution up to a maximum range of about 3-4 kms. Mounted on the back of a truck, it employs a pair of 2.4 m parabolic dish antennas easily deployed in remote locations and can be operated unattended for many days. Acquired data are processed in real time and are transferred to a host computer (PC) for display and recording. The FMCW was operated in IHOP_2002 in a vertically-pointing mode but has the ability to point in any direction.

An extended discussion of the FMCW is given by Ince et al. (2003). The FMCW images the Bragg backscattering from refractive index fluctuations due to isotropic turbulence which is related to the structure function parameter, C^2_n. In addition to Bragg scatter from clear air, return from Rayleigh point scatterers (non-refractive index scatterers), interpreted as insects, are possible and a subject of active current research (see Pollard et al, 2000).

Figure 10 shows the data for 22 May 2002 collected by the FMCW at Homestead, OK. In the figure, the radar echo is expressed in terms of the logarithm of the structure function, C^2_n, plotted at 2 sec resolution. The strong echo variations and the general trend of the echo tops reveal the convective plume updrafts and the growth and demise of the afternoon BL, respectively. The development of the boundary layer height with time reaching heights about 3.5km at its peak before collapsing down to 1.5 km after sunset (0140/2540 in the graph) is well characterized. Most interesting here is the coherent backscatter from surface to the top of

the CBL– plumes of enhanced structure function values mostly between 2000 and 2500. These higher values may be a result of an enhanced scatter of plumes of air as they rise in altitude. These coherent and enhanced signal levels are assumed to be primarily due to changes in temperature and moisture. A detailed look of these plumes reveals a variable width organization, wider at the base and narrowing with altitude with most of them reaching the 2 – 2.5 km level. The width of the base (in minutes) and the distance between each of these plume structures was variable and was better defined above 1.5 km. The duration in time of the plumes varied between about 2-9 minutes.

e. The Multiple Antenna Profiler Radar (MAPR)

The National Center for Atmospheric Research (NCAR) Atmospheric Technology Division (ATD) deployed an Integrated Sounding System (ISS) [Parsons et al, 1994] for the IHOP project. The ISS consisted of a standard surface meteorology station, a sodar, a radiosonde station, and a UHF wind profiler. The wind profiler used was MAPR (Multiple Antenna Profiler Radar, Cohn et. al. 1997, 2001), an advanced boundary layer radar based on a highly modified Radian (now Vaisala) LAP-3000 915 MHz wind profiler. Conventional wind profilers use one receiving antenna steered in multiple directions, however, MAPR uses four receiving channels, all directed vertically. This configuration allows the radar to make wind measurements on time periods as short as 30 seconds to five minutes, compared with 15 - 30 minutes for a conventional profiler. Another feature of the radar is that it can continuously monitor vertical motion allowing detailed study of boundary layer convection.

MAPR uses Spaced Antenna techniques (e.g., Briggs, 1984) to make horizontal wind measurements and comparisons with anemometers indicate that the uncertainties in

horizontal winds are about 1.5 m/s (Cohn et al 2001). Vertical motion is measured using the Doppler shift of signals received by the vertically directed antennas in the same manner as conventional wind profilers. The uncertainties in vertical velocity measurements using MAPR have not been examined in detail; however, they can be expected to be similar to that of conventional profilers. Angevine (1997), using conventional profilers, found that the most significant error in mean vertical velocity measurements of the convective boundary layer is a systematic bias downward of 0.1 - 0.3 m/s. This error is generally attributed to insects. The dominant scattering targets for UHF profilers are clear-air refractivity gradients such as that due to turbulence, however, these radars are also sensitive to echoes from insects and birds. Insects have been found to be good tracers for clear-air motion, with the exception of the downward bias in vertical velocity measurements.

MAPR measured winds continuously at Homestead, with a five-minute break every half hour to make RASS (Radio Acoustic Sounding System) virtual temperature measurements. The vertical resolution was typically 100 meters, although there were periods when the radar was operated in a mode capable of better than 20-meter vertical resolution (Yu and Brown, 2004). The time resolution of the vertical velocity measurements reported here is 30 seconds. The antenna beam width (full width half power) is about 8 degrees, which corresponds to a sampling volume 140 meters across at one-kilometer range. MAPR-measured vertical velocity on 22 May 2002, at Homestead Oklahoma, is shown in Figure 11.

f. The Atmospheric Emitted Radiance Interferometer (AERI)

The Atmospheric Emitted Radiance Interferometer (AERI) instrument is a fully automated ground-based interferometer which measures downwelling infrared radiation in discrete wavelengths (less than one wave number resolution) from 3.3 – 18 μm (Feltz, 2003). AERI

measures the radiance at better than 1% accuracy. The AERI-measured downwelling radiance spectra contain vertical temperature and water vapor profile information above the AERI instrument, as documented in Feltz et al. (1998) and Smith et al. (1999). Through inversion of the ill-posed radiative transfer equation, these profiles can be retrieved. However, because of the strength of the IR signal at the surface from emission within the lower atmosphere, the weighting functions become broad at 2.5–3.0 km, and thus the retrievals using only AERI data are limited to below this altitude. Geostationary Operational Environmental Satellite (GOES)-sounder temperature and moisture profiles are often combined with AERI measurements to extend the vertical reach, which is not done here. AERI comparisons with radiosondes have indicated absolute rms mixing ratio differences of 5%, and 1 K for temperature, at a resolution of 10-minute for IHOP operation.

Time–height cross sections of AERI derived water vapor mixing ratio, potential temperature and relative humidity data for 22 May 2002 are plotted in Fig. 9. The diurnal temperature and moisture trends are well represented. A drop in water vapor mixing ratio from 8-10 g/kg to 6 g/kg between 2140-2230 (as in the SRL data but smoothed at longer time scales) associated with an increased mixing of the temperature contours was observed. The BL in this region was also warmer in temperature by 1-2 degrees than the adjacent (pre-2100 and post-2300) regions, confirming the suggestion above from surface measurements. In the period 2130 – 0000, a number of localized vertical structures seen in the figure, in particular in the temperature plot, are hints of the convection organization on the day - (sub)sampled at a low (10-minute) resolution.

4. Analysis of the Homestead profile data

a. Moisture variability

In Fig. 13a, an overlay of the SRL measured water vapor mixing ratio with the FMCW derived structure function profile is shown. The SRL data is interpolated to FMCW times in this plot. A number of points can be readily made: i) The afternoon evolution of the BL height growth and the collapse just before sunset (~ 0140) show, in general, a similar *trend*, as captured by the 5 g/kg water vapor mixing ratio contour line for SRL (selected arbitrarily) and the overall echo strength of the FMCW. ii) Clouds – Cumulus clouds, were observed by SRL starting about 2130 and cloud base height was on average about 3 km (+/- 0.2 km). For nearly all the lidar observations of cloud base, there are underlying enhanced echo plumes in the FMCW data that do not extend to cloud base altitudes. The highest these plumes reach in the FMCW data is about 2.5 km. A similar moisture enhancement is observed in the SRL water vapor mixing ratio profile data coincident with the FMCW plumes. iii) A majority of the plumes from the FMCW corresponded, in time, to the plumes of moisture in the water vapor mixing ratio profiles from SRL. This is particularly true for altitudes higher than about 1 km. This is remarkable given that these two different data sets were sampled at two different resolutions: the FMCW radar data was collected at 2 sec temporal resolution while the SRL data, collected at 1 min intervals, was averaged to two (2.5?) minute temporal resolution.

A direct outcome of Fig. 13a is the determination of the "on" versus "off" plume moisture content. To accomplish this, the time of occurrence of the plumes using FMCW data was first determined and then the water vapor mixing ratio profile at that time selected from the SRL data. Note, however, that this characterization is limited to the SRL temporal resolution. Fortunately, the FMCW shows that a lot of these cores are more than a couple of minutes in duration (with majority of them in the 5-6 minute wide) and thus characterization of their moisture can be done adequately using the SRL profiles. For example, the average water

vapor mixing ratio calculated using the described method at a given altitude (2 km) for the updraft and downdraft cores was found 6.5 +/- 0.51 g/kg and 5.7 +/- 0.12 g/kg, respectively. This difference extended down to below 1 km level. To demonstrate that this plume structures extend the entire BL depth, we plot time series of mixing ratio data at 1.0, 1.5, 2.0, and 2.5 km altitudes (Fig. 13b) and the difference in mixing ratio amounts between successive data points (Fig. 13c: [i+1] – [i]) for each time series starting from 2100 to 2410, when clouds were present. The relative maxima and minima for all the levels corresponded in time – indicating coherent vertical structures of high and low water vapor mixing ratio plumes, respectively. The difference curves, a surrogate for difference between the updraft and downdraft core, varied roughly between 0.5 and -0.5, a difference of about 1 g/kg on average at the 2 km level. It becomes more difficult, however, to distinguish plumes boundaries in the FMCW data at the lower levels. An alternate method is the use of the cloud based as an indicator of the updraft plume, i.e. compare water vapor moisture directly under the cloud with mixing ratio profile in the immediate but cloud free environment. A demonstration of such a comparison is shown in Fig. 13d with more or less the same conclusion.

Another point to note in Fig 13b is the reversal in the temporal trend of water vapor mixing ratio at each altitude. The mixing ratio values at 2 km increased with time until about 2145 remaining constant for about 1 hr (2140 – 2230) before decreasing gradually as do the curves for all the levels except the time series taken from 1 km altitude. At 1 km altitude, the post 2230 trend was reversed: it shows an abrupt increase. Several processes may be at play here; in the pre-2140 time period convection dominated mixing moisture upward and thus leading to increase(decrease) of moisture at higher(lower) altitudes. Later, after sunset, the trend (gradual decrease) at higher elevations can be attributed to absence of convection, and thus

lack of surface moisture supply from below. However, at 1 km (low levels in general), advection associated with the north flowing cool/moist airmass dominated and led to wavy but increased moisture opposite the.

b. Vertical velocity data

An overlay plot of the MAPR derived vertical velocity data and the SRL measured water vapor mixing ratio is shown in Fig.14a. Data gaps in the MAPR data every half hour (in 5-minute duration) indicate times when the profiler was switched off in order to operate the RASS. In addition, the data is pruned and smoothed to remove many drop-out points. The 5-minute data gaps and the data dropouts complicate accurate visualization of the coherence in the updraft speed with altitude. Nevertheless, there are enough data points to ascertain that the updraft cores were observed throughout the BL. Although updraft speeds of up to about 3 m/sec were observed at the 1.5 km level around 2230, near the end of the dry intrusion over Homestead (Fig. 3 and 6) and near the stronger radar reflectivity fine line (main dryline), the bulk of the data was between -1 and 1 m/sec. Note that these values may be biased down by 0.1-0.3 m/sec overall due to influence attributed to insects, as described above. Note also updraft vertical velocities of up to 8-9 m/sec are reported by Weiss et al (2004) using a different approximation technique.

A comparison of the change between subsequent time series data points at altitudes 1.0, 1.5, 2.0, 2.5 km, both in mixing ratio and vertical velocity from SRL and MAPR (dashed curve), are plotted in Fig 14b. Difference between updraft and downdraft speeds were between 0.5 and -0.5 m/sec prior to about 2300 but decreased later (Fig. 14b). While the majority of changes are in phase, a number of out of phase peaks and dips are observed throughout the record. A better match between the mixing ratio and vertical velocity data is observed in the

time ranges 2100-2130, 2200-2230, and 2300-2330 and the match seems poorer after 2300. A combination of data gaps and dropout points, which have not been interpolated or corrected in any way may, have contributed towards this ambiguity in Fig. 14b. Nevertheless, it is clear that the majority of the updrafts were associated with increased moisture at all the levels during the highly convective part of the afternoon.

d. Boundary layer height variability:

Most ground based, as well as airborne, lidars profile in the vertical but a more representative spatial coverage is desired for a better representation of the spatial variability. HARLIE offers an advantage in looking at the "spatial" variability of the boundary layer height (BLH). Rotating continuously in Azimuth, it provides spatial sampling over several square km for boundary layer height variability (through the aerosol backscatter gradient) among many other products, that can be averaged and compared with traditional vertical lidar measurements or can be analyzed for BLH variability over time and space.

Fig. 15 shows a new way of quantifying the variability of the BLH on 22 May 2002. Plotted are BLH determined from the HARLIE aerosol backscatter measurements using a wavelet-based analysis (see Davis et al., 2000) and the standard deviation determined from the point measurements of HARLIE BLH based on each scan (about 36 profiles per scan). The BLH appears constant during the moist intrusion (2140-2230) but increased steadily throughout the rest of the afternoon with a slight bump noticeable just prior to 2300 (near the eastern dryline convergence zone). The BLH standard deviation prior reveals a local minimum at about 2230; with an apparent decrease prior to this time associated with the dry and warmer airmass while the increasing trend associated with the retrogression of the eastern dryline zone. This

is indicative of the vigorous mixing taking place around the dryline zone as observed by other instruments and discussed above. The advantage of these measurements is that the CBL activity can be quantified using the BLH standard deviation. The standard deviation varied between 50 m and 450 m corresponding to near sunset and late afternoon dryline boundary conditions, respectively. A difference of about 150 m was also observed between the maximum standard deviation of the BLH on both sides of the dryline convergence zone.
The BLH varied between 2.8 to 3.8 with most of the higher values coming from 2230 and later times when Homestead was located east of the dryline and large spatial and temporal variability within the HARLIE cone (5.5 -7.6 km radius at BLH ranges).

Starting at about 2400, an hour before sunset, a dramatic drop in the standard deviation signaled the turning-off the convection leading to the dissipation of the Cumulus clouds. An approaching upper-level cloud and the residual layer complicated the post 2515 BLH retrievals and a reliable height for the nocturnal boundary layer cannot be obtained on this day, a well known problem for nighttime application of backscatter lidars. An extended analysis of the movement of the dryline and detailed statistics of the BLH is being done and will be published elsewhere.

5. SUMMARY

Measurements made by an array of instrument platforms made during a dryline condition that occurred in western Oklahoma on 22 May 2002 during the International H2O Project (IHOP). The paper primarily presents the data sets collected by the ground based lidar and radar profilers at the profiler site in the Oklahoma Panhandle that we refer here as Homestead. These data sets are augmented by data collected from conventional surface and upper-air observations as ell as aircraft based lidar and radar instrumentation. Although refinements of

the many data sets still continue, several unique observations of the 22 May 2002 dryline evolution can be made and are presented here. Several mobile radars and an armada of mobile-mesonet instrumentation were also deployed on this day which are the subject of two other papers in this volume.

The data collected on 22 May 2002 dryline reveals that at synoptic scales the environment was typical of many other drylines reported (see for example Schaefer, 1986). Cool and moist air to over much of the west-central Oklahoma was capped by a temperature inversion overlaid by a well-mixed, dry and warm airmass. The inversion in far western Oklahoma began to erode, following sunrise, and mixing of dry air aloft with low level moist air. GOES satellite maps on this day revealed an approaching cold front north of the profiling site where it interacted with a the dryline marked by a wedge of Cumulus clouds. These clouds formed a wedge shaped pattern that was visible between 2100 and 0030, covering much of the Texas-Oklahoma Panhandle and the profiling site widening southward and appearing stationary. At Homestead, first indications of the dryline were made about 1600 (about one hour before noon) – shown as a gradual increase in the GPS-measured precipitable water vapor amounts from a constant of about 1.5 cm to about 3 cm. The dryline also appeared to be quasi-stationary until early afternoon (2130) but started to move east later until about 2230 when it reversed direction again. As it did, a wedge-shaped and well-mixed boundary layer started to emerge separating a very dry region to the west and a moist region to the east – leading to two convergence zones. A unique feature of this case was the emergence of the double-dryline convergence zones leading to three different regions. Although Homestead and the many mobile IHOP instrumentation for the day were far south than where the convection was triggered, they were ideally located to capture this unique feature of the double-dryline

evolution, vertical structure, organization of the Cu forming convection, and the sharp moisture contrasts that occurred.

The lidars-observed afternoon boundary layer revealed a highly variable moisture organization at Homestead: starting with an average of bout 8-9 g/kg water vapor mixing ratio in the lowest one km and dropping abruptly to 6-7 g/kg and a well-mixed convective boundary layer (0-3 km) and changing back once again to a more environment at low levels (up to 12 g/kg). These changes were related to the east-and-then-west movements of the dryline on this day and the moisture contrasts are mainly between the wedge-shaped airmass and the air east of the main (eastern) dryline convergence zone. The driest far western region did not move east far enough over Homestead to be sampled by the profiling instruments, but aircraft measurements revealed water vapor mixing ratio values of less than 4 g/kg at 1.6 km – equivalent to values recorded at altitude of 3.5 km and above at Homestead. The water vapor mixing ratio measurement near the main, eastern, dryline convergence zone showed a highly variable moisture organization ranging anywhere from 2 to 7 km. The variability within this convective boundary layer was well documented using a new scanning lidar technique that quantified the small scale (6-7 km wide) horizontal variability of the boundary layer height (BLH). The peak-to-peak variation of the standard deviation of the BLH within about a radius of 6-7 km around Homestead varied from a low of about 250 m when the dry well-mixed region was over Homestead (~2230) to about 450 m when the dryline was retrograding and immediate east of the main dryline convergence zone. The BLH standard deviation was also a better indicator of the CBL activity than the aerosol backscatter or the aerosol scattering ratio which the later two failed to capture the nocturnal BLH duet to complications introduced by the residual layer and other reasons. The day-night transition in BLH activity was reflected in the standard deviation values reasonably: decreasing steadily

from about 400 m at about 2340 (two hours before sunset) to about 50 m (an hour before sunset).

Aircraft based lidar measurements also suggest and support earlier findings (McCarthy and Koch, 1982; Parsons et al. 1991) that the boundary is not straight but wavy – with 10-20 km intrusions of moist air into the dry side in as short a distance as 3 km. The vertical moisture stratification became well defined as the night progressed. Starting about an hour before sunset, the convective activity ceased leading to an almost homogenous and moister layer of about 1.5 km deep transitioning to a dry region aloft. A prominent feature of the this transition interface is the gently slopped (eastward tilted) moisture bulge found at the leading edge followed by dip (about 0.5 km) and smaller amplitude waves that follow. Lidar derived wind speed profiles show a similarly slopped decrease along the moisture slope followed by an increase in wind speed at the time of the dip. A noticeable shift in wind direction from about south-southwest to south-southeast throughout the depth of the moist layer was noted. These findings are in agreement with numerous previous findings (Schaefer 1986; Hane et al. 1993; Ziegler et al. 1995; Shaw et al. 1997; Hane et al. 1997; Atkins et al. 1998; Parsons et al. 2000). They are a striking visualization of the advective nature of the nocturnal flow and the effect of the flow reversal within the moist air and subsequent convergence with the western flow associated with a retrograding dryline. Moisture lifting at the leading edge followed by a strong subsidence (Weiss and Bluestein, 2002; Weiss et al. this volume) leading to decrease in mixing ratio values as a result of drier air intrusion from above the moist layer.

Simultaneous analysis of the radar, profiler and lidar data revealed that the dryline convergence zone was populated by updraft plumes of about 5-6 minutes wide (up to 7 km wide at 14-16 m/sec wind speed) rising to cloud base. The updrafts and downdrafts were

harder to distinguish from the data sets at low altitudes but were distinct at higher altitudes, probably because a greater contrast existed between the sinking and rising airmass. These allowed for easier identification of the updraft boundaries and confidence in assigning moisture, speed and other thermodynamic quantities. Updraft plumes were moister than the surrounding and in many cases topped by a Cumulus cloud. They posses an average moisture excess of about 1 g/kg than their surroundings at 2 km height and through most of the lower boundary layer. Updraft speeds of about 3 m/sec were observed at 1.5 km level near the main dryline convergence zone by both the ground based profiler and the UWKA in-situ probes. Higher instantaneous values of vertical velocity speeds were present in the profiler data. These values are much lower than the 8-9 m/sec reported by Weiss et al (2004 and same authors in this volume) using a pseudo-multiple Doppler radar techniques in the same general area for the same dryline case.

6. ACKNOWLEDGEMENT

This research was sponsored by the National Science Foundation (NSF) and the National Aeronautical and Space Administration (NASA).

7. REFERENCES

Angevine, W.M., 1997: Errors in mean vertical velocities measured by boundary layer wind profilers, *J. Atmos. Ocean. Tech.*, 14, 565-569.

Atkins, N. T., R. M. Wakimoto, and C. L. Ziegler, 1998: Observations of the finescale structure of a dryline during VORTEX 95: *Mon. Wea. Rev.*, **126**, 525-550.

Bluestein, H. B., 1993: CLASS for class. *Bull. Amer. Meteor. Soc.*, **74**, 1697–1702.

——, and S. S. Parker, 1993: Modes of isolated, severe convective storm formation along the dryline. *Mon. Wea. Rev.*, **121,** 1354–1372.

Bruneau, D., P. Quaglia, C. Flamant, M. Meissonnier, and J. Pelon, 2001: Airborne lidar LEANDRE II for water-vapor profiling in the troposphere. *Applied Optics*, **40**, 3450-3475.

Cohn, S.A., W.O.J. Brown, C.L. Martin, M.S. Susedik, G. Maclean, and D.B. Parsons, 2001: Clear air boundary layer spaced antenna wind measurement with the Multiple Antenna Profiler (MAPR), *Annales Geophys.*, **19**, 845-854.

Cohn, S.A., C.L. Holloway, S.P. Oncley, R.J. Doviak, and R.J. Lataitis, 1997: Validation of a UHF spaced antenna wind profiler for high-resolution boundary layer observations, *Radio Sci.*, **32**, 1279-1296.

Crook, A., 1996: Sensitivity of moist convection forced by boundary layer process to low level thermodynamic fields. *Mon. Wea. Rev.*, **124**, *1767-85.*

Davis, K. J., N. Gamage, C. R. Hagelberg, C. Kiemle, D. H. Lenschow, and P. P. Sullivan, 2000: An Objective Method for Deriving Atmospheric Structure from Airborne Lidar Observations. *J. Atmos. Oceanic Technol.*, **17**, 1455-1468.

Demoz, B.B., D.O'C. Starr, D.N. Whiteman, K.D. Evans, and D. Hlavka, 2000: Raman LIDAR detection of cloud base, *Geophys. Res. Lett.*, Vol **27**, No. 13, 1899-1902.

Di Girolamo, P., R. Marchese, D. N. Whiteman, B. B.Demoz (2004), Rotational Raman Lidar measurements of atmospheric temperature in the UV, *Geophys. Res. Lett.*, **31**, L01106, doi:10.1029/2003GL018342.

Fabry, F., 2004: Meteorological value of ground target measurements by radar. *J. Atmos. Oceanic Technol.*, **21**, 560-573.

Feltz, W. F., H. B. Howell, R. O. Knuteson, H. M. Woolf, and H. E. Revercomb, 2003: Near continuous profiling of temperature, moisture, and atmospheric stability using the Atmospheric Emitted Radiance Interferometer (AERI), *J. Appl. Meteor.*, **42**, 584-597.

Feltz, W. F., W.L. Smith, R. O. Knuteson, H. E. Revercomb, H. M. Woolf, H. B. Howell, 1998: *J. Appl. Meteor.*, **37**, 857-875.

Fujita, T. T., 1958: Structure and movement of a dry front. *Bull. Amer. Meteor. Soc.*, **39**, 574–582.

Geerts, B. and Q. Miao, 2004: Vertical velocity bias of echo plumes in the convective boundary layer, detected by an airborne mm-wave radar. *J Atm Ocean Tech*, Submitted (nov 03)

Gentry, B., H Chen and S. X. Li, 2000: Wind Measurements with a 355 nm Molecular Doppler Lidar *Optics Letters*, **25**, 1231-1233.

Hane, C. E., C. L. Ziegler, and H. B. Bluestein, 1993: Investigation of the dryline and convective storms initiated along the dryline: Field experiments during COPS-91. *Bull. Amer. Meteor. Soc.*, **74**, 2133-2145.

Hane, C. E., H. B. Bluestein, T. M. Crawford, M. E. Baldwin, and R. M. Rabin, 1997: Severe thunderstorm development in relation to along-dryline variability: A case study. *Mon. Wea. Rev.*, **125**, 231–251.

Ince, T., et al., 1998: A high resolution FMCW S-band radar for boundary layer profiling and cloud applications. *Proceedings, Battlespace Atmospherics Conference*, Hanscom AFB, MA, 1998, 43-439.

Koch, S. E., and J. McCarthy, 1982: The evolution of an Oklahoma dryline. Part II: Boundary-layer forcing of mesoconvective systems. *J. Atmos. Sci.*, **39,** 237–257.

Martin, W. J. and M. Xue (2004): Initial condition sensitivity analysis of mesoscale forecast using very large Ensembles, Preprint- *84th AMS annual Meeting, Seattle, Washington, 11-15 January 2004*

McCarthy, J., and S. E. Koch, 1982: The evolution of an Oklahoma dryline. Part I: A meso- and subsynoptic-scale analysis. *J. Atmos. Sci.*, **39,** 225–236.

National Severe Storms Project (NSSP Staff), 1963: Environmental and thunderstorm structures as shown by National Severe Storms Project observations in spring 1960 and 1961. *Mon. Wea. Rev.*, **91,** 271–292.

Parsons, D.B., W. Dabbert, H. Cole, T. Hock, C. Martin, A.L. Barrett, E. Miller, M. Spowart, M. Howard, W. Ecklund, D. Carter, K. Gage and J. Wilson, 1994: The Integrated Sounding System: Description and preliminary observations from TOGA COARE, . *Bull. Amer. Meteor. Soc.*, **98**, 553-567.

Parsons, D.B., M. A. Shapiro, and E. R. Miller, 2000: The mesoscale structure of a nocturnal dryline and of a frontal-dryline merger. *Mon. Wea. Rev.*, **128**, 3824-3838.

Parsons, D. B., M. A. Shapiro, R. M. Hardesty, R. J. Zamora, and J. M. Intrieri, 1991: The finescale structure of a west Texas dryline. *Mon. Wea. Rev.*, **119,** 1283–1292

Pollard, b., S. Khanna, S. J. Frasier, J. C. Wygaard, D. W. Thomson, R. E. McIntosh, 2000: Local structure of the convective boundary layer from a volume-imaging radar. *J. Atmos. Sci.*, **57,** 2281-2296.

Rhea, J. O., 1966: A study of thunderstorm formation along the dryline. *J. Appl. Meteor.*, **5,** 58–63.

Schaefer, J. T., 1974: The life cycle of the dryline. *J. Appl. Meteor.*, **13,** 444–449.

——, 1986: The dryline. *Mesoscale Meteorology and Forecasting,* P. S. Ray, Ed., Amer. Meteor. Soc., 549–572.

Shaw, B. L., R. A. Pielke, and C. L. Ziegler, 1997: A three-dimensional numerical simulation of a Great Plains dryline. *Mon. Wea. Rev.*, **125,** 1489–1506.

Sun, W. Y., 1987: Mesoscale convection along the dryline. *J. Atmos. Sci.*, **44,** 1394–1403.

——, and Y. Ogura, 1979: Boundary layer forcing as a possible trigger to a squall line formation. *J. Atmos. Sci.*, **36,** 235–254.

Schwemmer, G., T. Wilkerson, and D. Guerra, 1998: Compact scanning lidar systems using holographic optics. *SPIE Conf. Optical Remote Sensing for Industry and Environmental Monitoring*, Beijing,

Schwemmer, G.K., 1998: Holographic Airborne Rotating Lidar Instrument Experiment, *19th International Laser Radar Conference*, NASA/CP-1998-207671/PT2, pp. 623-626, Annapolis, Maryland, 6-10 July 1998.

Shaw, B. L., R. A. Pielke, and C. L. Ziegler, 1997: A three-dimensional numerical simulation of a Great Plains dryline. *Mon. Wea. Rev.*, **125**, 1489-1506.

Smith, W. L., W. E. Feltz,, R. O. Knuteson, H. E. Revercomb, H. M. Woolf, H. B. Howell, 1998: The retrieval of planetary boundary layer structure using ground-based infrared spectral radiance measurements. *J. Atmos. Oceanic Technol* ., **16**, 323-333.

Weckwerth, T. M., 2000: The effect of small-scale moisture variability on thunderstorm initiation. *Mon. Wea. Rev.*, **128**, 4017-4030.

Weckwerth, T. M., C. R. Pettet, F. Fabry, S. Park and J. W. Wilson, 2004: Radar refractivity retrieval: Validation and application to short-term forecasting. *J. Appl. Meteor.*, submitted.

Weckwerth, T. M. D. B. Parsons, S. E. Koch, J. A. Moore, M. A. LeMone, B. B. Demoz, C. Flamant, B. Geerts, J. Wang and W. F. Feltz, 2003: An overview of the International H_2O Project (IHOP_2002) and some preliminary highlights. *Bull. Amer. Meteor. Soc.*, **85**, 253-277.

Weckwerth, T.M., J.W. Wilson and R.M. Wakimoto, 1996: Thermodynamic variability within the convective boundary layer due to horizontal convective rolls. *Mon. Wea. Rev.*, **124**, 769-784.

Weiss, C. C., and H. B. Bluestein, 2002: Airborne pseudo-dual Doppler analysis of a dryline-outflow boundary intersection. *Mon. Wea. Rev.*, **130**, 1207-1226.

Weiss, C. C., and H. B. Bluestein, 2004: Fine-scale Radar observations of a dryline during the International H2O project. Preprint- *84th AMS annual Meeting, Seattle, Washington, 11-15 January 2004*

Wilkerson, T. D., I. Q. Andrus, G. K. Schwemmer, D. O. Miller, 2001:Horizontal Wind Measurements using the HARLIE Holographic Lidar, *Proceedings of SPIE Vol.4484 Optical Remote Sensing for Industry and Environment Monitoring II*, San Diego, California, 30-31 July 2001).

Whiteman, D. N., S. H. Melfi, 1999: Cloud liquid water, mean droplet radius and number density measurements using a Raman lidar, *J. Geophys. Res.*, **104** No. D24, 31411-31419.

Whiteman, David N., 2003: Examination of the traditional Raman lidar technique. I. Evaluating the temperature-dependent lidar equations, *Applied Optics*, **42**, No. 15, 2571-2592.

Whiteman, David N., 2003: Examination of the traditional Raman lidar technique. II. Evaluating the ratios for water vapor and aerosols, *Applied Optics*, **42**, No. 15, 2593-2608

Whiteman, D. N., K. D. Evans, B. Demoz, D. O'C. Starr, E. Eloranta, D. Tobin, W. Feltz, G. J. Jedlovec, S. I. Gutman, G. K. Schwemmer, M. Cadirola, S. H. Melfi, F. J. Schmidlin,

2001: Raman lidar measurements of water vapor and cirrus clouds during the passage of hurricane Bonnie, *J. of Geophys. Res.*, **106**, No. D6, 5211-5225.

Whiteman, D. N., S. H. Melfi, 1999: Cloud liquid water, mean droplet radius and number density measurements using a Raman lidar, *J. Geophys. Res.*, **104** No. D24, 31411-31419.

Whiteman, D. N., S. H. Melfi, R. A. Ferrare, 1992: Raman Lidar System for Measurement of Water Vapor and Aerosols in the Earth's Atmosphere, *Appl. Opt.*, **31** No. 16 3068 - 3082.

Yu, T.-Y. and W.O.J. Brown, 2004: High-resolution atmospheric profiling using combined spaced antenna and range imaging techniques, *Radio Science*, **39**(1), RS1011.

Ziegler, C. L., W. J. Martin, R. A. Pielke, and R. L. Walko, 1995: A modeling study of the dryline. *J. Atmos. Sci.*, **52**, 263-285.

Ziegler, C. L., and C. E. Hane, 1993: An observational study of the dryline. *Mon. Wea. Rev.*, **121**, 1134–1151.

——, and E. N. Rasmussen, 1998: The initiation of moist convection at the dryline: Forecasting issues from a case study perspective. *Wea. Forecasting*, **13**, 1106–1131.

——, W. J. Martin, R. A. Pielke, and R. L. Walko, 1995: A modeling study of the dryline. *J. Atmos. Sci.*, **52**, 263–285.

——, T. J. Lee, and R. A. Pielke, 1997: Convective initiation at the dryline: A modeling study. *Mon. Wea. Rev.*, **125**, 1001–1026.

FIGURE CAPTIONS

Figure 1. Satellite observations and surface map at 2200 and 1900 UTC on 22 May 2002. The IHOP profiling site, location of the Spol radar (arrows), aircraft flight paths (P3 and UWKA), the ARM CART site, IHOP flux stations and Lear jet dropsonde locations are indicated. Note the wedge of popcorn cumulus clouds in the Texas and Oklahoma panhandle – about 11 miles wide around the IHOP ground sites. Surface station observations for the IHOP domain at 1900 are also sown (bottom).

Figure 2. Surface-based measurements of temperature, water vapor mixing ratio, precipitable water vapor, refractive index (both the wet and dry term), wind speed and direction on 22 May 2002 at the IHOP profiling site. An expanded view of the data when the lidars were operational is also shown. Note that the temperature scale is reversed for the expanded view.

Figure 3: Radiosonde plots of temperature, dew point temperature and wind direction from three locations: at IHOP profiling site (within the Cumulus cloud region), just west of the site (in the cloud free region) and just east of the site. Not that the driest sonde is associated with winds from 200 degrees.

Figure 3b. A cross section of water vapor mixing ratio and potential temperature from ground (Homestead, and Mobil groups by NCAR and NSSL) and aircraft (Lear Jet) released radiosondes across (W-E) the dry line. See Fig.1 for the locations of the dropsondes. Location of the UW King Air leg at 1.6 km (discussed below) and lidar derived cloud base are also shown. A well defined transition is revealed at the top of the dryline in the west-central Oklahoma. However, the cumulus cloud region is characterized by substantial mixing of the moisture up to about 3.8 km. N.B. Not drawn to scale. The Lear jet dropsonde release points (L1-L8) have a separation of about 30-40 km while the first three ground based sonde profiles are separated by 13 km and 18 km,

Figure 4. Top: Time sequence (2101, 2200, 2300, 0000) of reflectivity, near-surface refractivity, 5-min surface refractivity change obtained by the NCAR S-pol radar and surface wind collected over the IHOP profiling site. The distance rings for the reflectivity and refractivity are shown at 20, 40, and 60 km and only the 20 km ring is shown in the 5-min refractivity change panel. Bottom: time series of refractivity at Homestead derived from surface observation (black), from SRL and AERI measurements at 0.5 km (blue) and from S-pol at 2.5 km are plotted. Location of the IHOP profiling site (black dote) and the dryline convergence zones (D1, D2) as well as regions of different airmass are indicated.

Figure 5. Water vapor mixing ratio and vertical velocity (dotted curve) data collected by in-situ probes aboard the UWKA. Values shown are for a single leg at 1.6 km as UWKA flew from NNW-to-SSE across the field of cumulus clouds (its relative location is shown in fig. 3.). Note that the vertical velocity SSE of D1 decrease abruptly and is on the average negative. The change in water vapor mixing ratio across the dryline convergence zones and the relative distance between the two transitions are indicated.

Figure 6. (A) Water vapor mixing ratio (g/kg) profile measured by the LEANDREII on the NRL P-3 on a E-W flight leg about 3-4km to the south of the IHOP profiling site (see Fig. 1). The lidar was pointed horizontally from P-3 (at 1 km - 1.2 km AGL) on this flight leg. An

unfortunate L2 operation led to the unfortunate data gap (A) right about the eastern dryline convergence zone. (B) Time series comparison of the integrated L2 and in-situ P3 water vapor mixing ratio data. Approximate positions of the IHOP Profiling site (H) and relevant boundaries as well as some distance scales are also shown.

Figure 7. GLOW measurements of the wind speed and direction on 22 May 2002 at the IHOP profiling site. A curve outlining the boundaries of wind speed decrease is overlaid on the wind direction panel - visualizing that behind the wind speed decrease (top) is a hint of a "jet" associated with the southerly wind flow. Note the gap in the x-axis when sector scans at different elevation were made in order to detect variations in the dryline associated flows (not shown here).

Figure 8. HARLIE backscatter profiles showing location of the cumulus clouds, afternoon growth of the BL and the nighttime demise. HARLIE operated in profile mode till about 2140 UTC and switched to conical scanning afterwards, thus the data gap.

Figure 9. Time-height plot of the SRL measured water vapor mixing ratio (g kg-1) at the IHOP profiling site on 22 May 2002. Note the location of the clouds shown by the base of white strips (on average about 3.3 km), the drier and well mixed BL intrusion between 2140 – 2230 (R2), the structure of the eastern dryline convergence zone (D1), the moist airmass east of the dryline (R2) and the approximate sunset time.

Figure 10. Time-height plot of the FMCW measured structure function at the IHOP Profiling site on 22 May 2002. Also penciled in are the relative locations of average cloud base altitude derived from lidar, the eastern dryline convergence zone (D1) and the air mass on both sides of the eastern dryline region (R1, R2) as well as the sunset time.

Figure 11. Vertical velocity (m/sec) observed by the NCAR MAPR/ISS on 22 May 2002 at the IHOP profiling site. The relative locations of average cloud base altitude derived from lidar, the eastern dryline convergence zone (D1) and the air mass on both sides of the eastern dryline region (R1, R2) as well as the sunset time are indicated.

Figure 12. AERI retrieved profiles of water vapor mixing ratio (top) and potential temperature (bottom) at the IHOP profiling site on 22 May 2002 and the approximate locations of the eastern dryline convergence boundary and associated regions.

Figure 13. a) An overlay of time-height water vapor mixing ratio (contour) from the SRL and refractivity profiles from the FMCW (background). Note the time-matched mixing ratio and reflectivity updraft cores (vertical intrusions). b) Examples of time series water vapor mixing ratio data at 1, 1.5, 2, 2.5 km and c) the mixing ratio change with time. d) Examples of profiles of mixing ratio from "on" and "off" the plumes in (a), showing cloud location and the difference in mixing ratio.

Figure 13. a) An overlay of time-height water vapor mixing ratio (contour) from the SRL and refractivity profiles from the FMCW (background). Note the time-matched mixing ratio and reflectivity updraft cores (vertical intrusions). b) Examples of time series water vapor mixing ratio data at 1, 1.5, 2, 2.5 km and c) the mixing ratio change with time. d) Examples of profiles of mixing ratio from "on" and "off" the plumes in (a), showing cloud location and the difference in mixing ratio.

Figure 14. *Top:* An overlay of MAPR and SRL measurements: Note the updraft intensity at 2230-2300 and at 2430-2500 associated with the eastern dryline zone (D1) and the nighttime moisture hump prior to sunset. *Bottom:* Time series change (w_{t+1}-w_t) of vertical velocity and mixing ratio at 1, 1.5, 2, 2.5 km

Figure 15. HARLIE derived boundary layer heights and standard deviation of the boundary layer height on 22 May 2002 at the IHOP profiling site.

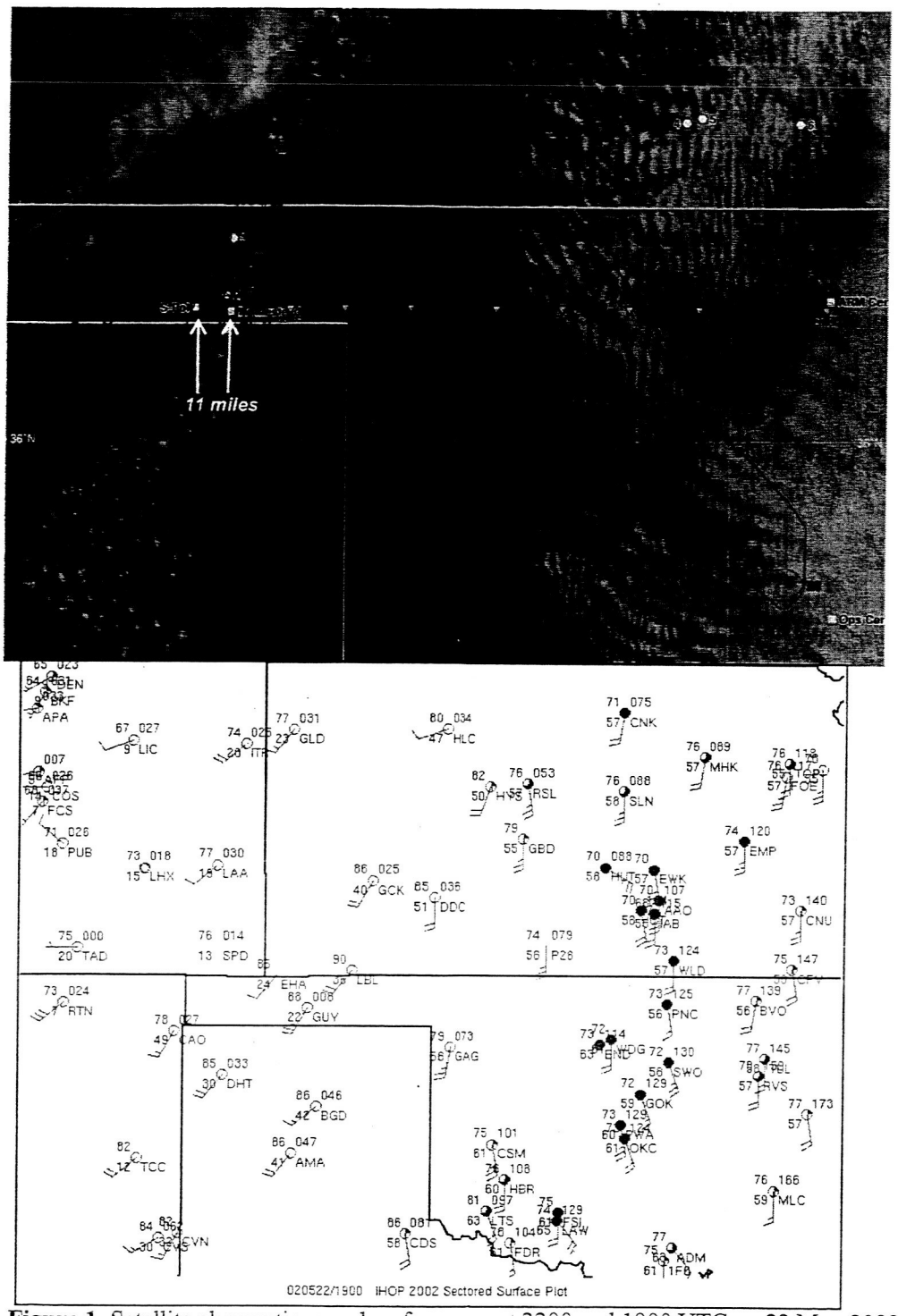

Figure 1. Satellite observations and surface map at 2200 and 1900 UTC on 22 May 2002. The IHOP profiling site, location of the Spol radar (arrows), aircraft flight paths (P3 and UWKA), the ARM CART site, IHOP flux stations and Lear jet dropsonde locations are indicated. Note the wedge of popcorn cumulus clouds in the Texas and Oklahoma panhandle – about 11 miles wide around the IHOP ground sites. Surface station observations for the IHOP domain at 1900 are also sown (bottom).

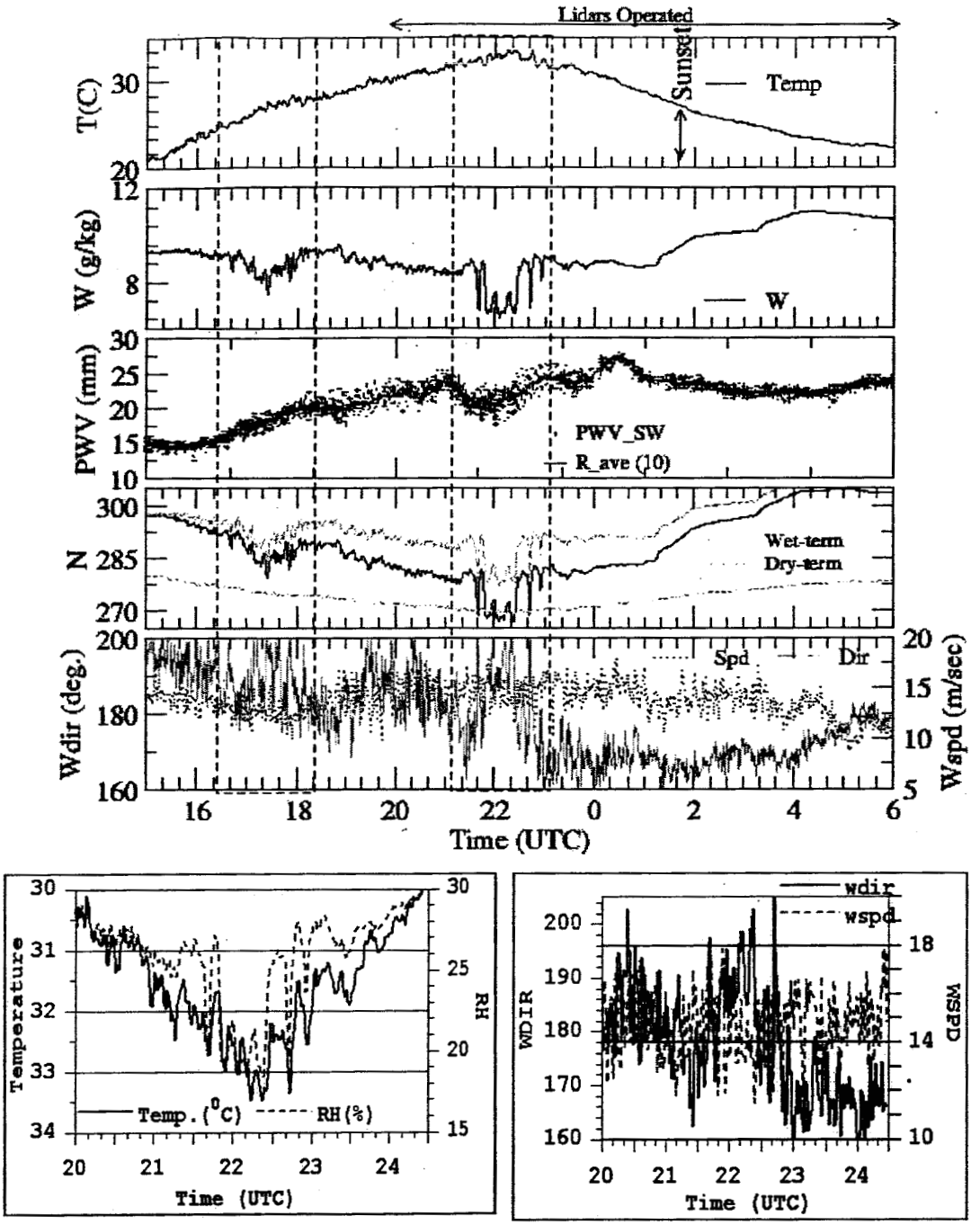

Figure 2. Surface-based measurements of temperature, water vapor mixing ratio, precipitable water vapor, refractive index (both the wet and dry term), wind speed and direction on 22 May 2002 at the IHOP profiling site. An expanded view of the data when the lidars were operational is also shown. Note that the temperature scale is reversed for the expanded view.

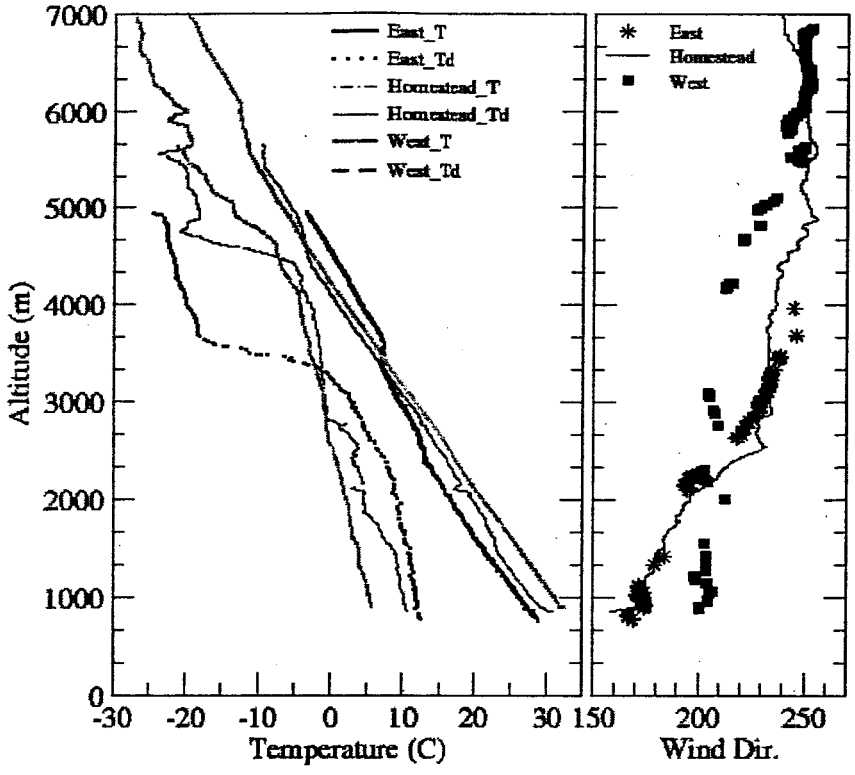

Figure 3: Radiosonde plots of temperature, dew point temperature and wind direction from three locations: at IHOP profiling site (within the Cumulus cloud region), just west of the site (in the cloud free region) and just east of the site. Not that the driest sonde is associated with winds from 200 degrees.

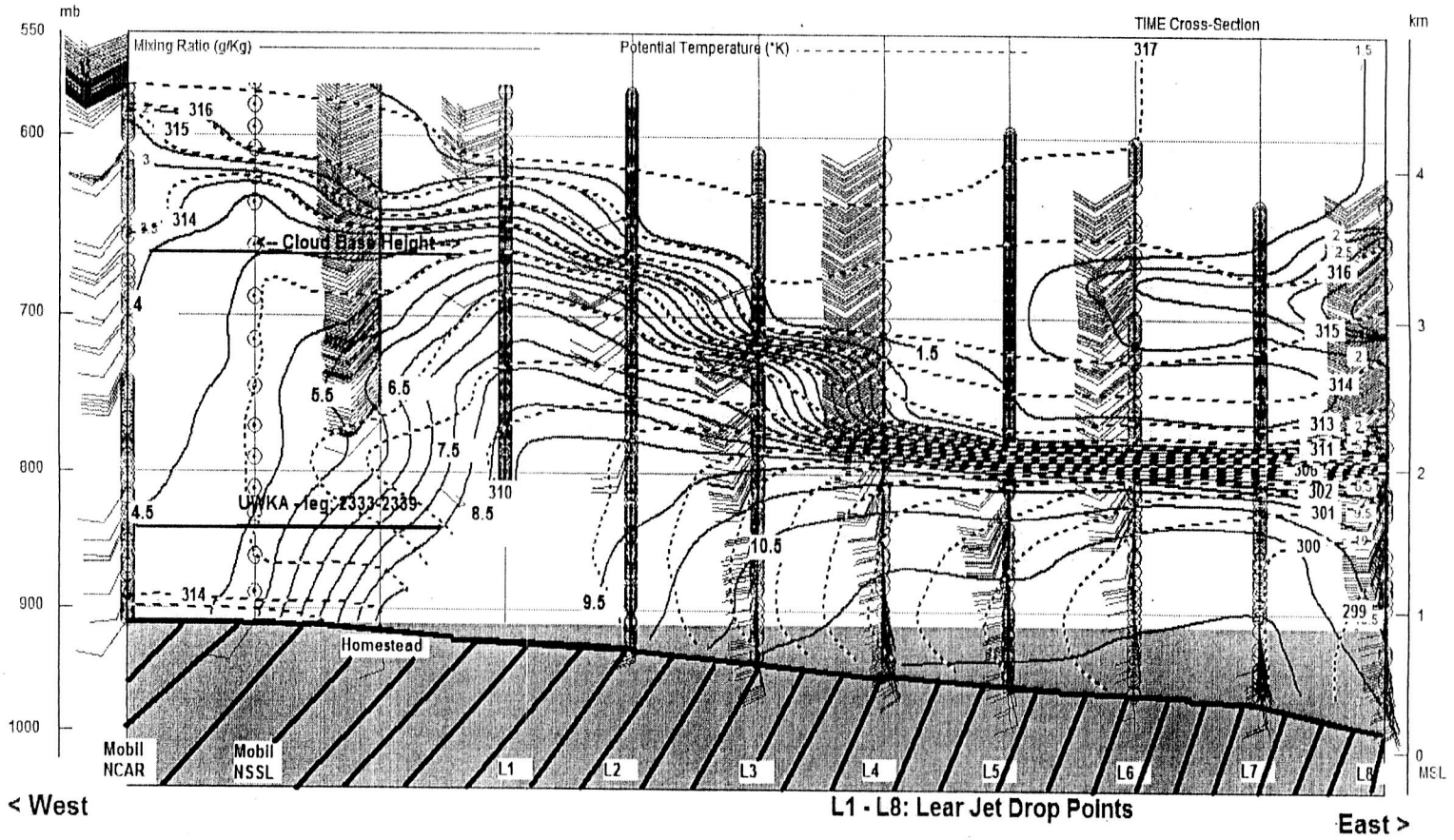

Figure 3b. A cross section of water vapor mixing ratio and potential temperature from ground (Homestead, and Mobil groups by NCAR and NSSL) and aircraft (Lear Jet) released radiosondes across (W-E) the dry line. See Fig.1 for the locations of the dropsondes. Location of the UW King Air leg at 1.6 km (discussed below) and lidar derived cloud base are also shown. A well defined transition is revealed at the top of the dryline in the west-central Oklahoma. However, the cumulus cloud region is characterized by substantial mixing of the moisture up to about 3.8 km. N.B. Not drawn to scale. The Lear jet dropsonde release points (L1-L8) have a separation of about 30-40 km while the first three ground based sonde profiles are separated by 13 km and 18 km,

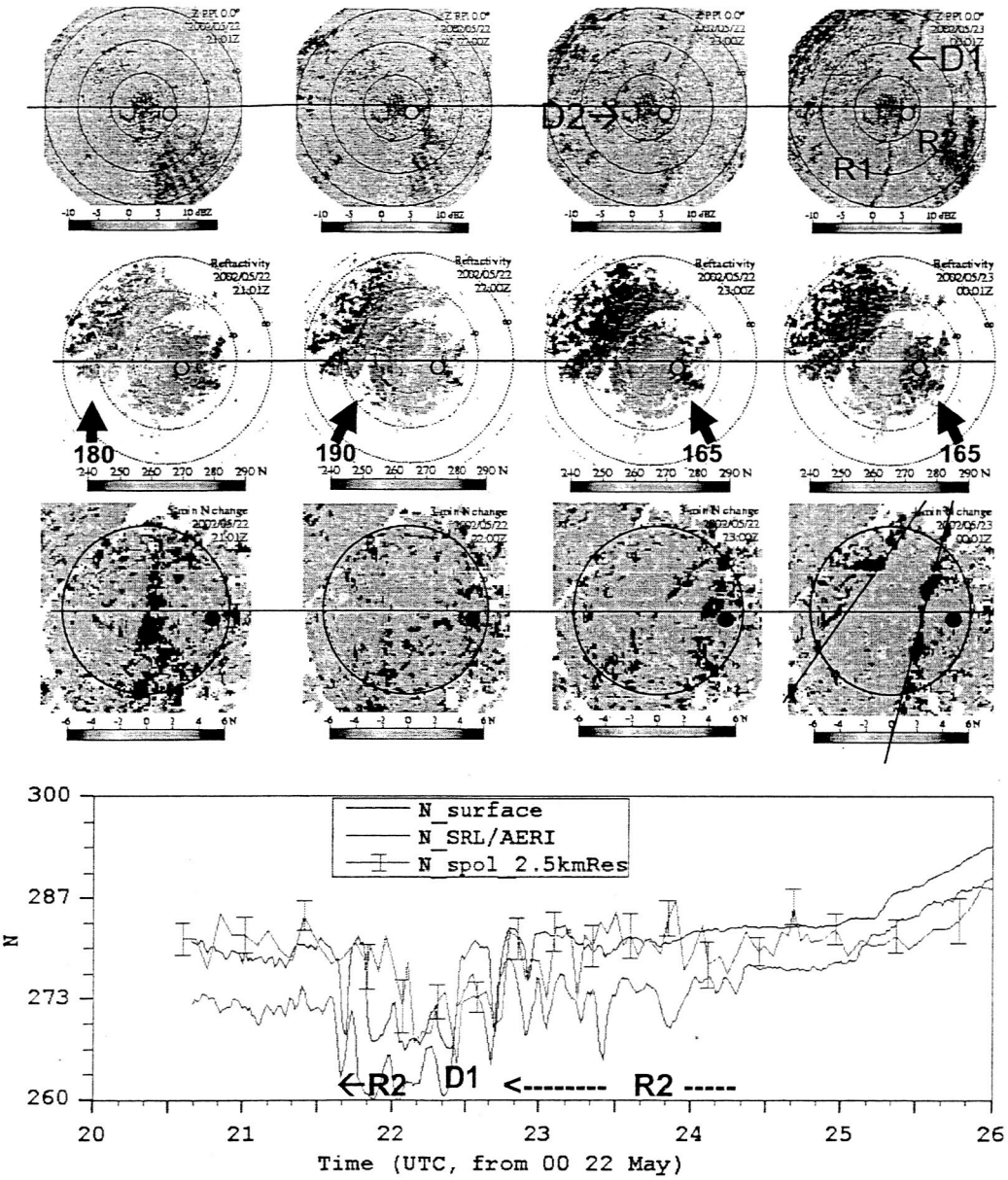

Figure 4. Top: Time sequence (2101, 2200, 2300, 0000) of reflectivity, near-surface refractivity, 5-min surface refractivity change obtained by the NCAR S-pol radar and surface wind collected over the IHOP profiling site. The distance rings for the reflectivity and refractivity are shown at 20, 40, and 60 km and only the 20 km ring is shown in the 5-min refractivity change panel. Bottom: time series of refractivity at Homestead derived from surface observation (black), from SRL and AERI measurements at 0.5 km (blue) and from S-pol at 2.5 km are plotted. Location of the IHOP profiling site (black dote) and the dryline convergence zones (D1, D2) as well as regions of different airmass are indicated.

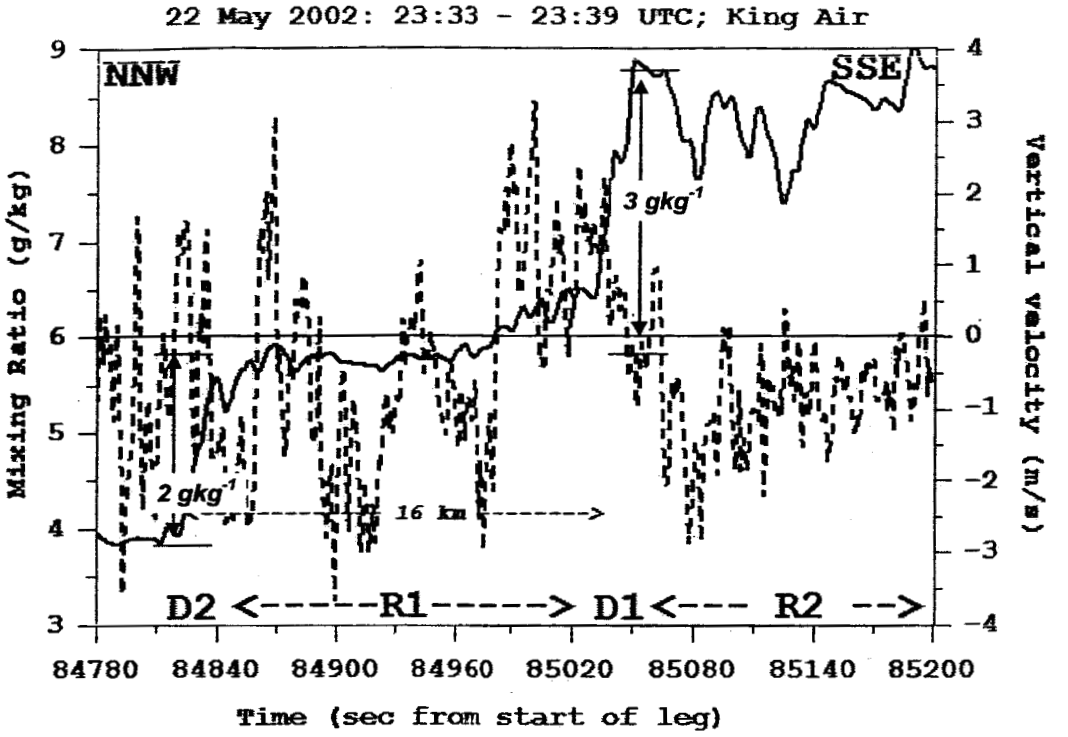

Figure 5. Water vapor mixing ratio and vertical velocity (dotted curve) data collected by in-situ probes aboard the UWKA. Values shown are for a single leg at 1.6 km as UWKA flew from NNW-to-SSE across the field of cumulus clouds (its relative location is shown in fig. 3.). Note that the vertical velocity SSE of D1 decrease abruptly and is on the average negative. The change in water vapor mixing ratio across the dryline convergence zones and the relative distance between the two transitions are indicated.

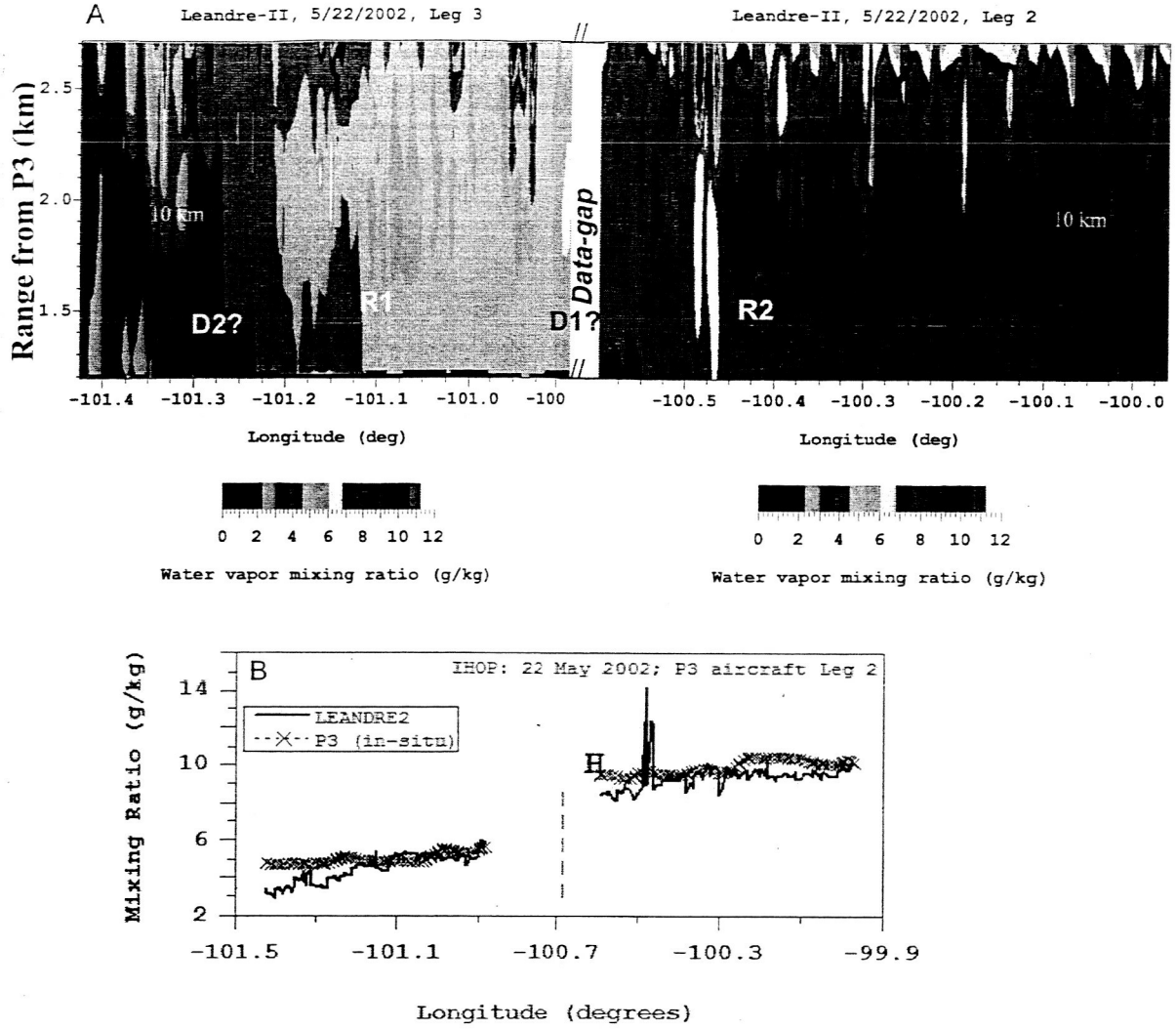

Figure 6. (A) Water vapor mixing ratio (g/kg) profile measured by the LEANDREII on the NRL P-3 on a E-W flight leg about 3-4km to the south of the IHOP profiling site (see Fig. 1). The lidar was pointed horizontally from P-3 (at 1 km - 1.2 km AGL) on this flight leg. An unfortunate L2 operation led to the unfortunate data gap (A) right about the eastern dryline convergence zone. (B) Time series comparison of the integrated L2 and in-situ P3 water vapor mixing ratio data. Approximate positions of the IHOP Profiling site (H) and relevant boundaries as well as some distance scales are also shown.

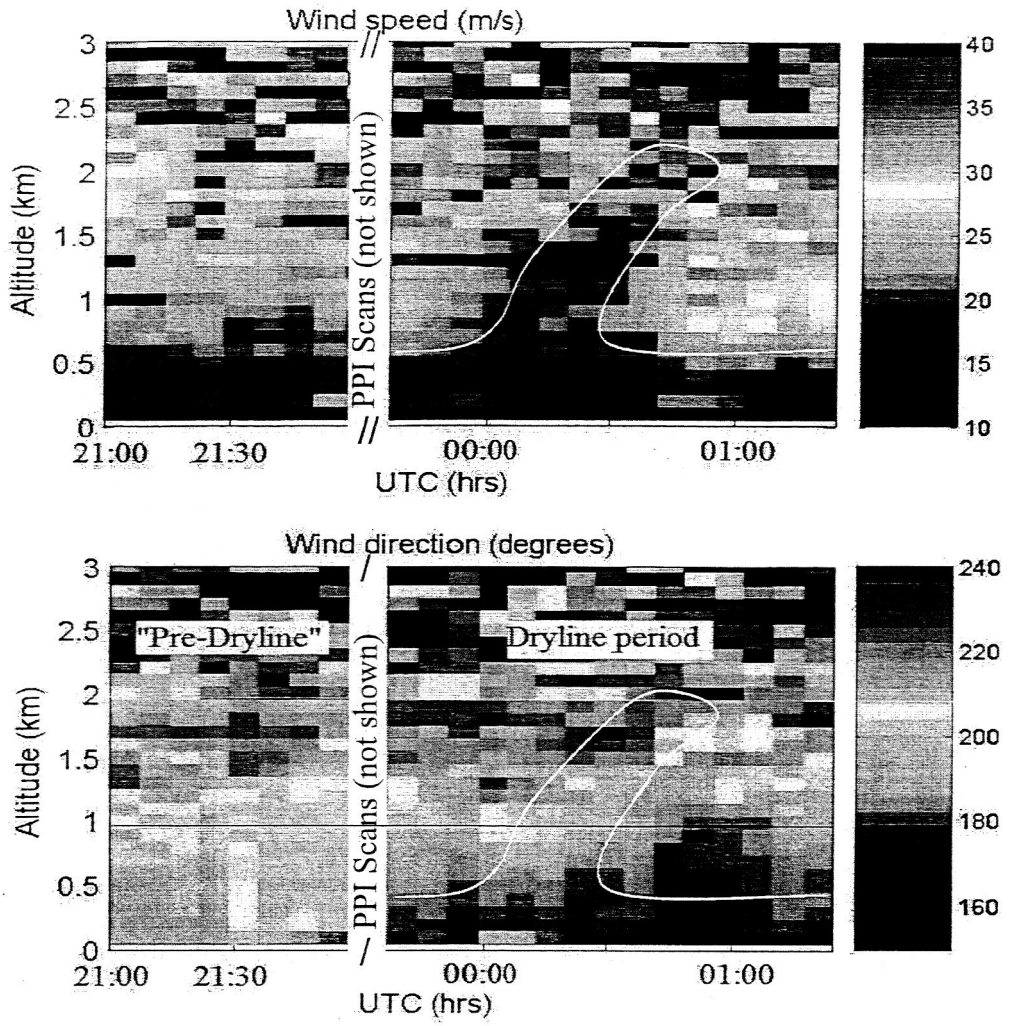

Figure 7. GLOW measurements of the wind speed and direction on 22 May 2002 at the IHOP profiling site. A curve outlining the boundaries of wind speed decrease is overlaid on the wind direction panel - visualizing that behind the wind speed decrease (top) is a hint of a "jet" associated with the southerly wind flow. Note the gap in the x-axis when sector scans at different elevation were made in order to detect variations in the dryline associated flows (not shown here).

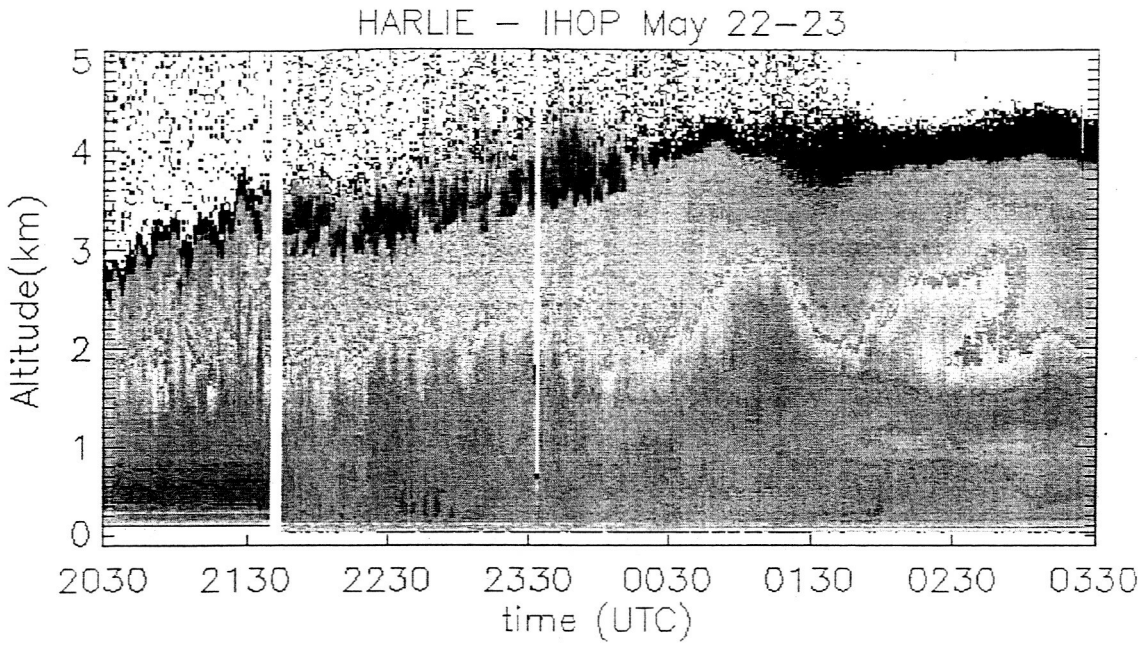

Figure 8. HARLIE backscatter profiles showing location of the cumulus clouds, afternoon growth of the BL and the nighttime demise. HARLIE operated in profile mode till about 2140 UTC and switched to conical scanning afterwards, thus the data gap.

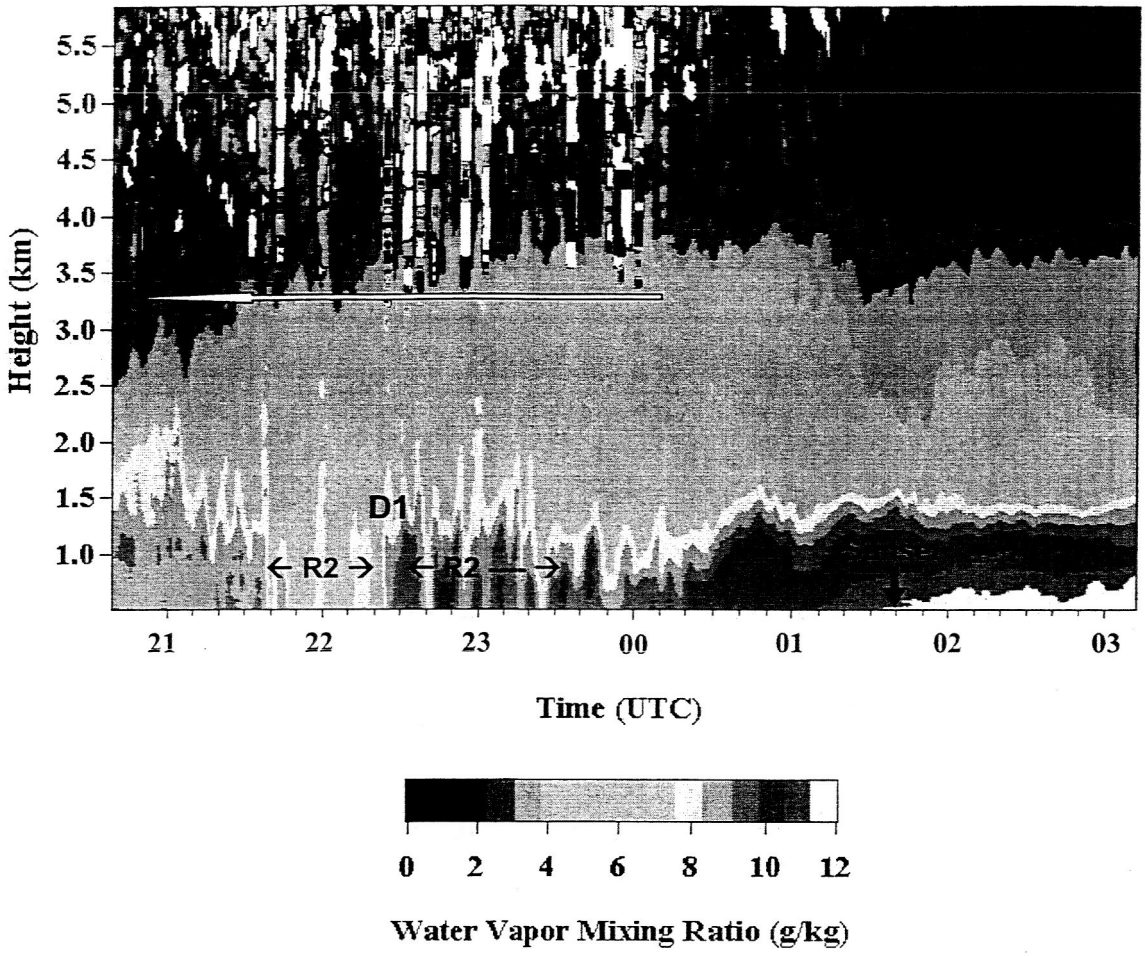

Figure 9. Time-height plot of the SRL measured water vapor mixing ratio (g kg-1) at the IHOP profiling site on 22 May 2002. Note the location of the clouds shown by the base of white strips (on average about 3.3 km), the drier and well mixed BL intrusion between 2140 – 2230 (R2), the structure of the eastern dryline convergence zone (D1), the moist airmass east of the dryline (R2) and the approximate sunset time.

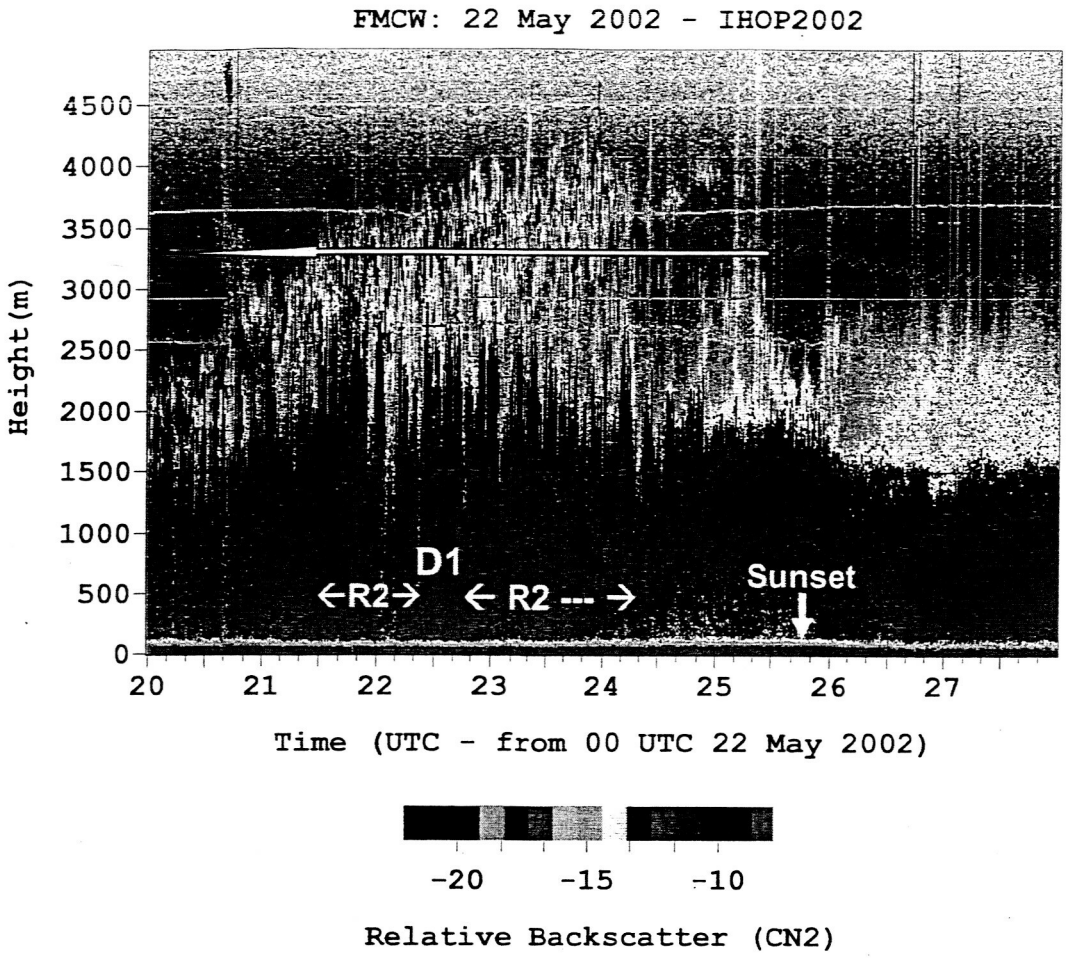

Figure 10. Time-height plot of the FMCW measured structure function at the IHOP Profiling site on 22 May 2002. Also penciled in are the relative locations of average cloud base altitude derived from lidar, the eastern dryline convergence zone (D1) and the air mass on both sides of the eastern dryline region (R1, R2) as well as the sunset time.

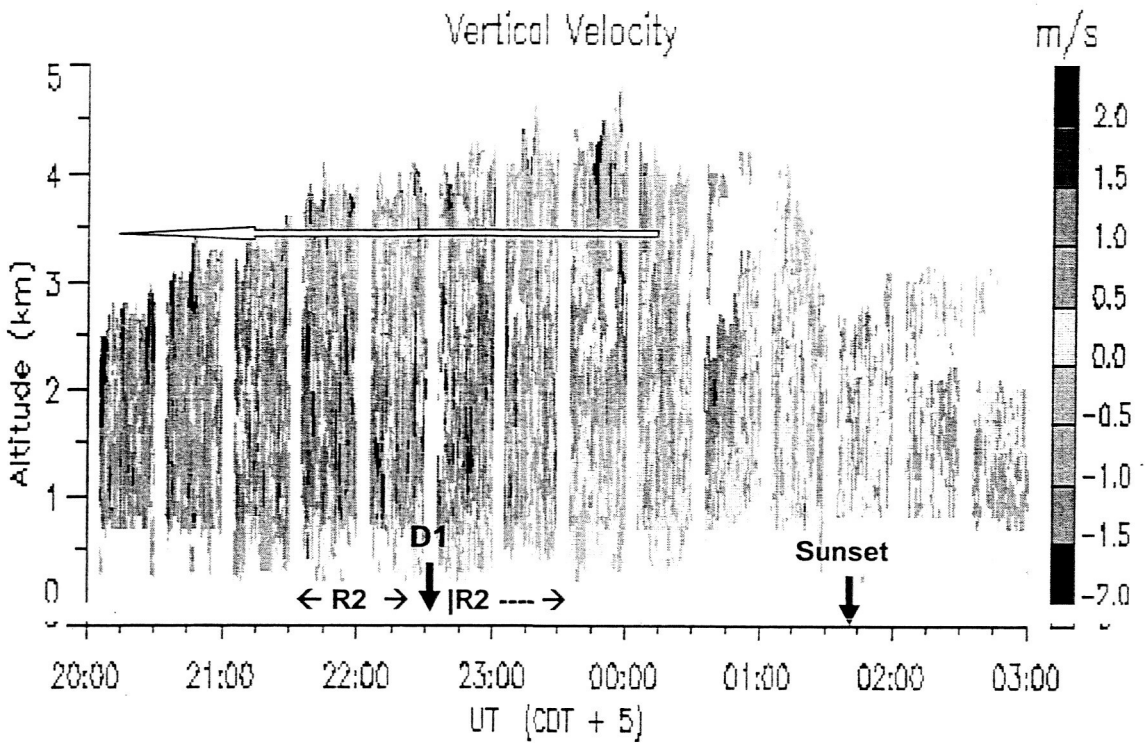

Figure 11. Vertical velocity (m/sec) observed by the NCAR MAPR/ISS on 22 May 2002 at the IHOP profiling site. The relative locations of average cloud base altitude derived from lidar, the eastern dryline convergence zone (D1) and the air mass on both sides of the eastern dryline region (R1, R2) as well as the sunset time are indicated.

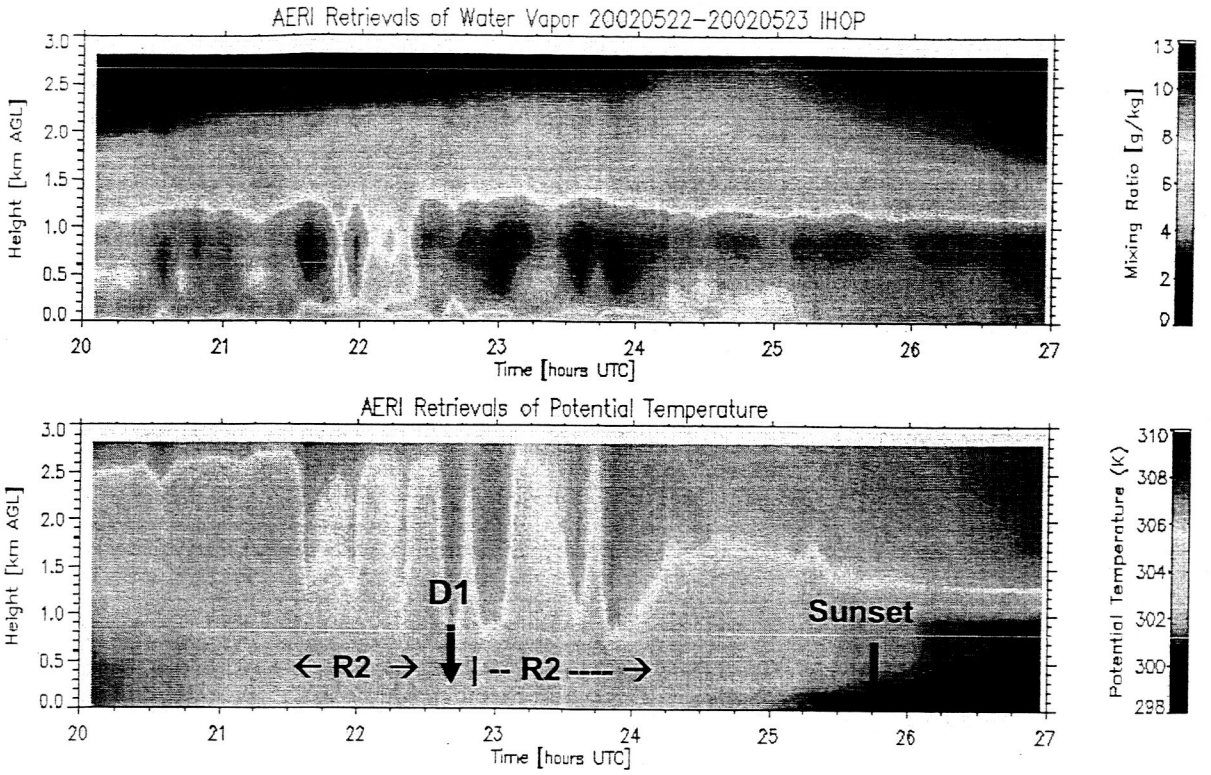

Figure 12. AERI retrieved profiles of water vapor mixing ratio (top) and potential temperature (bottom) at the IHOP profiling site on 22 May 2002 and the approximate locations of the eastern dryline convergence boundary and associated regions.

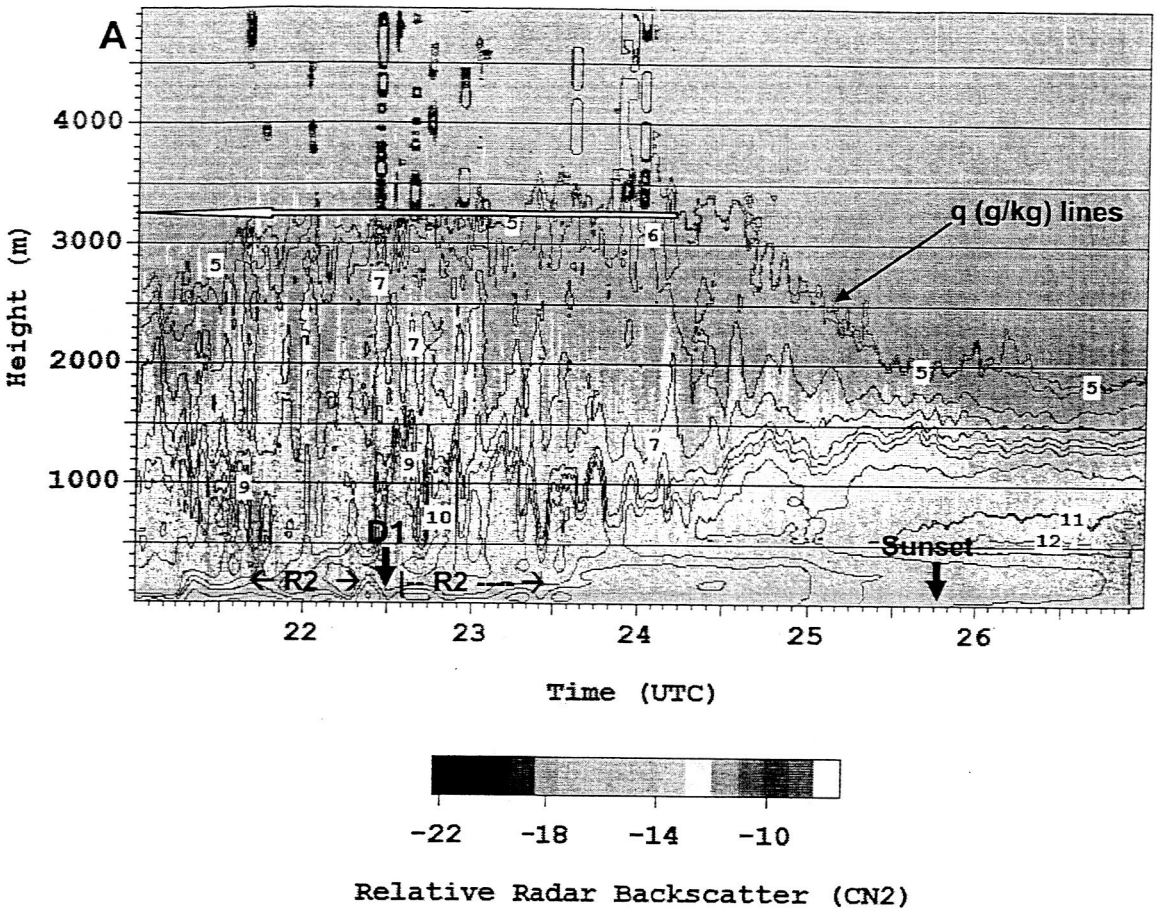

Figure 13. a) An overlay of time-height water vapor mixing ratio (contour) from the SRL and refractivity profiles from the FMCW (background). Note the time-matched mixing ratio and reflectivity updraft cores (vertical intrusions). b) Examples of time series water vapor mixing ratio data at 1, 1.5, 2, 2.5 km and c) the mixing ratio change with time. d) Examples of profiles of mixing ratio from "on" and "off" the plumes in (a), showing cloud location and the difference in mixing ratio.

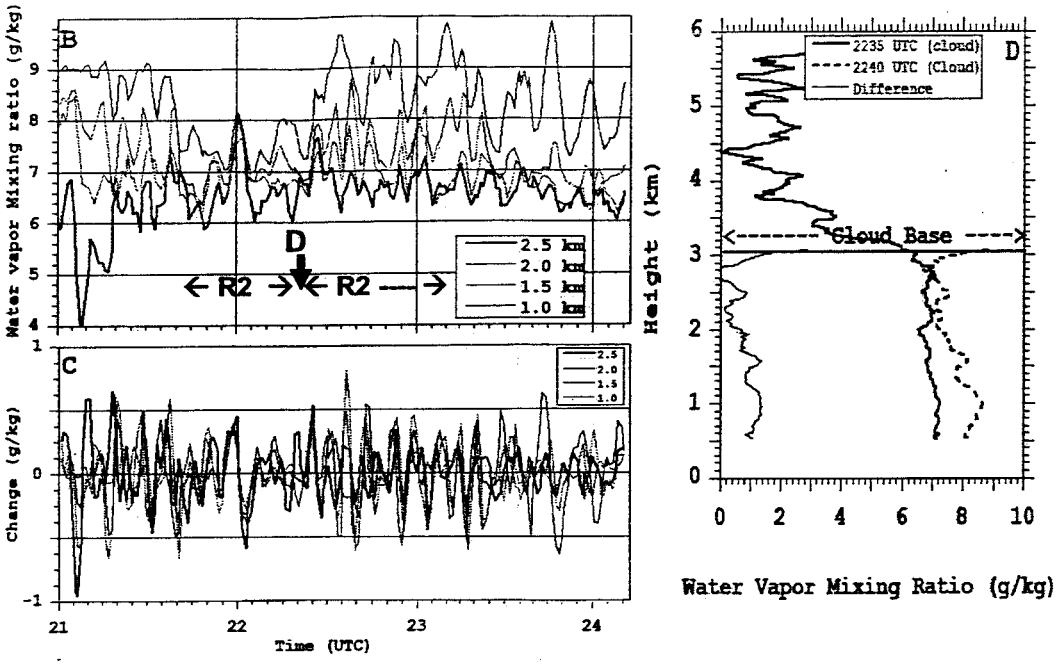

Figure 13. a) An overlay of time-height water vapor mixing ratio (contour) from the SRL and refractivity profiles from the FMCW (background). Note the time-matched mixing ratio and reflectivity updraft cores (vertical intrusions). b) Examples of time series water vapor mixing ratio data at 1, 1.5, 2, 2.5 km and c) the mixing ratio change with time. d) Examples of profiles of mixing ratio from "on" and "off" the plumes in (a), showing cloud location and the difference in mixing ratio.

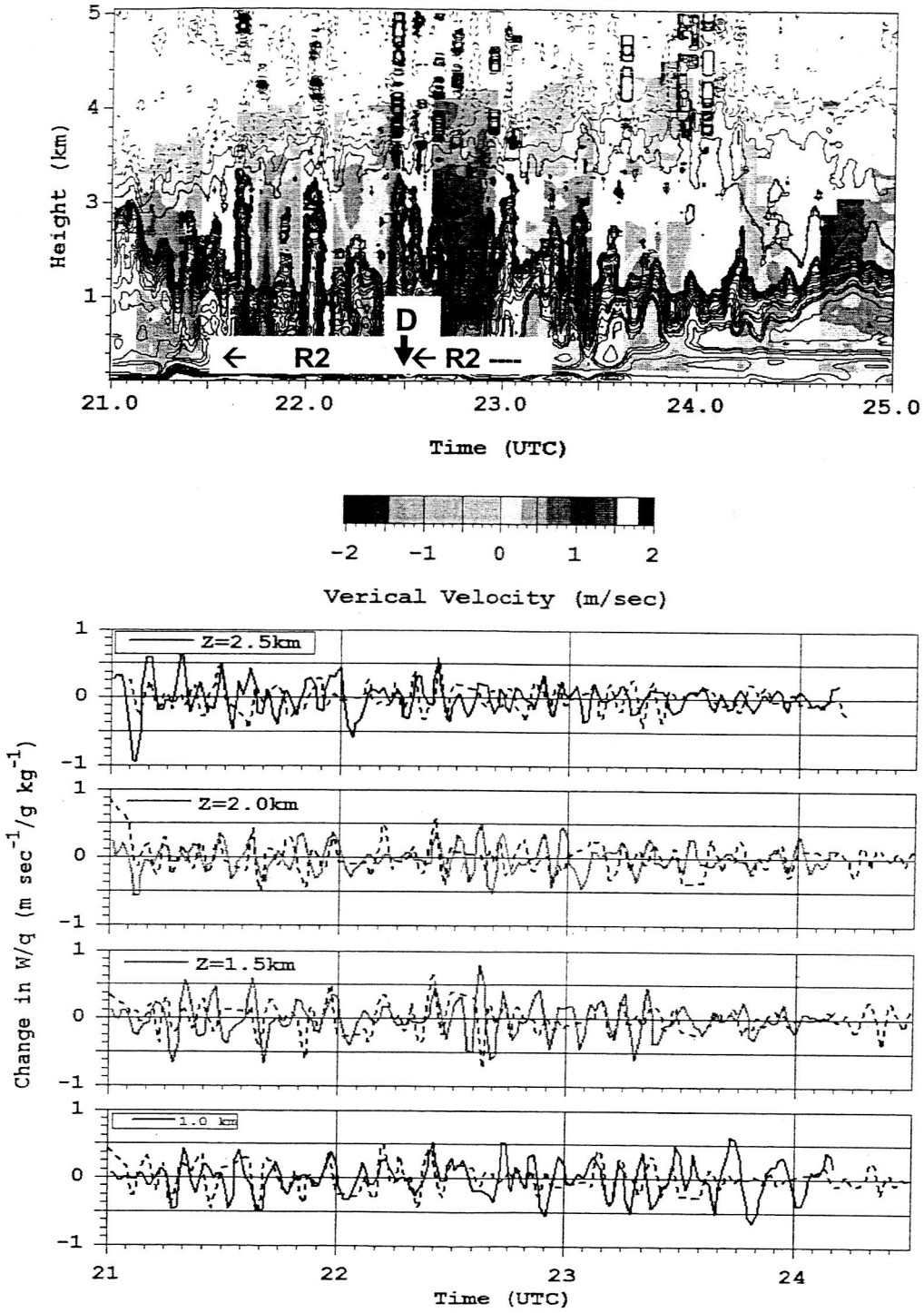

Figure 14. Top: An overlay of MAPR and SRL measurements: Note the updraft intensity at 2230-2300 and at 2430-2500 associated with the eastern dryline zone (D1) and the nighttime moisture hump prior to sunset. Bottom: Time series change (w_{t+1}-w_t) of vertical velocity and mixing ratio at 1, 1.5, 2, 2.5 km.

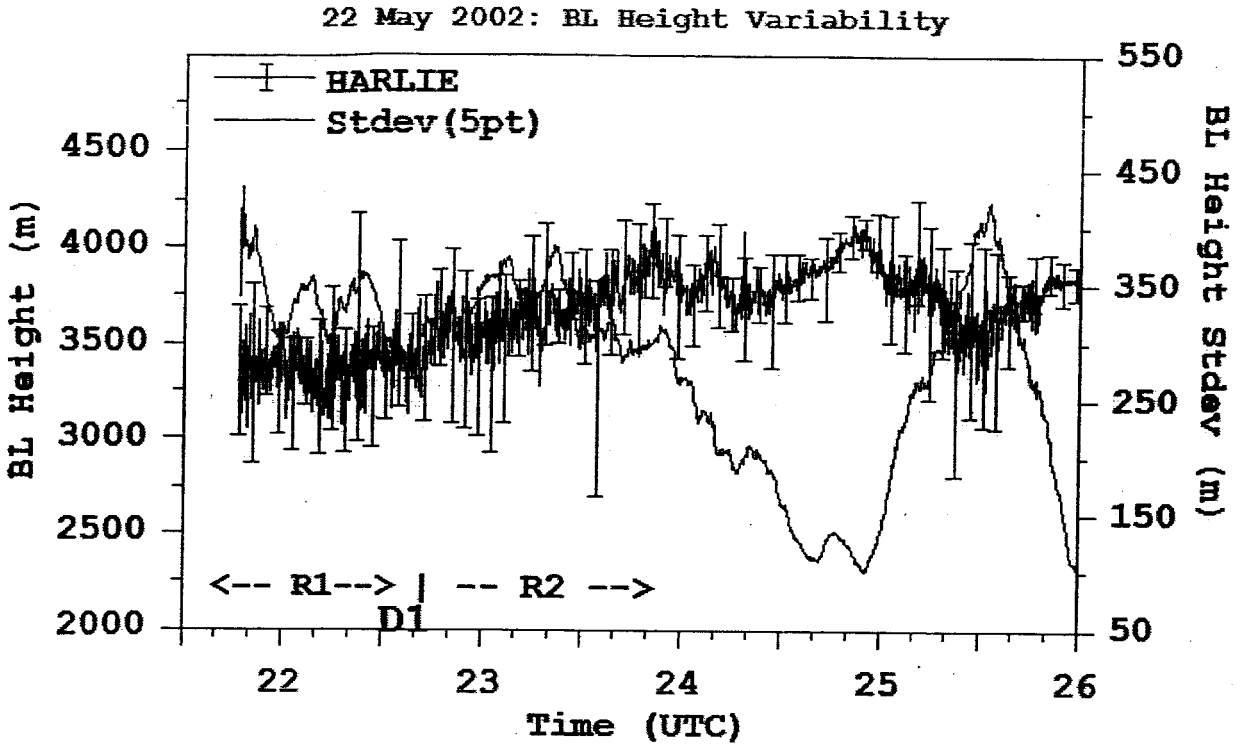

Figure 15. HARLIE derived boundary layer heights and standard deviation of the boundary layer height on 22 May 2002 at the IHOP profiling site.